A Comparative and Exploratory Study of Homogeneous and Inhomogeneous Stratified Turbulence

by

Dinesh Siewnarine

A thesis
presented to the University of Waterloo
in fulfillment of the
thesis requirement for the degree of
Master of Mathematics
in
Applied Mathematics

Waterloo, Ontario, Canada, 2021

Author's Declaration

I hereby declare that I am the sole author of this thesis. This is a true copy of the thesis, including any required final revisions, as accepted by my examiners.

I understand that my thesis may be made electronically available to the public.

Abstract

The study of turbulence in the oceans and atmosphere is far-flung and ever-reaching in the academic world with research being done theoretically, experimentally and numerically. With great strides in the increasing power of numerical computation over the years, forced and/or stratified homogeneous turbulence has been studied extensively for multiple simulation setups which give situational results for the inertial range as well as the energy power-law relationships. Some experimental examples are seen in such setups as raking a tank filled with uniformly saline water or the application of some dye to investigate internal wave propagation. On the other hand, numerical simulations often strive to explain certain behaviours by predominantly varying the Reynolds and Froude numbers but a myriad of literature also exists that employs the use of the Richardson and Prandtl numbers as well.

One property that homogeneous turbulence does not wholly capture is that of global intermittency. Turbulent regions occur as patches or clouds in nature and there have been few pieces of literature that investigate this inhomogeneity of stratified turbulence and how it behaves when left to freely decay without any forcing. Within this study, a turbulent cloud is numerically set up within an otherwise quiescent cubic domain to represent an inhomogeneous turbulent region. Using a similarly sized cubic domain, the entirety of it is used to model homogeneous turbulence. Then, using direct numerical simulations, a comparison of the non-forced, freely decaying evolution of homogeneous and inhomogeneous turbulence is established where results strive to provide an introductory investigation for the development of a turbulent cloud. This study looks into the evolution of energy, length scales, Froude and buoyancy Reynolds numbers as well as energy spectra within the cloud along with a focus on wave presence and energy of the inhomogeneous system outside of the cloud. It has been found that the shape of the cloud and the initial stratification used in the simulations play a critical role in the evolution of the cloud and large stratification indicates to the presence of highly energetic waves propagating at angles near to the outside edges of the cloud.

Acknowledgements

ācāryadevo bhava

Unfathomable gratitude is to be dedicated to the supervisor of this thesis, Professor Michael Waite, who has been a unshakeable pillar of clarity, patience, understanding, sound advice and inspiration during this course of study. It is a stroke of immensely great fortune to have had the opportunity to work with a professor of such calibre and it certainly has been a tremendous experience to be under his guidance.

Sincerest thanks must also be given to Professors Marek Stastna and Francis Poulin for not only agreeing to be part of the defence committee but also for exhibiting the beauty of Applied Mathematics through their taught courses as well as being ever available for words of guidance about this study.

Much appreciation must also be directed towards Jesse Legaspi, Kwan Lai, James Lowman and Martin Magill for all their constant help, counsel and cheer.

It should also be mentioned the office-mates during this time of study who facilitated in an engaging and jubilant atmosphere to work in.

To the Applied Mathematics department at the University of Waterloo, who were ever swift and diligent in administrative tasks and quality of courses offered, contributed with the others above to ensure an enjoyable program and amicable workplace.

This work was facilitated in part by the computing powerhouse that is SHARCNET and Compute Canada.

Dedication

To family, friends and well-wishers who have always been there every step of the way and constantly lit up the path forward.

Table of Contents

List of Figures

List of Tables

Chapter 1

Introduction

Within this thesis, a comparative and exploratory but also idealized study of homogeneous and inhomogeneous stratified turbulence is undertaken which finds application and relevance to both the atmosphere and oceans. The main method through which this research is done is numerical in nature but it is of tantamount importance that the theoretical understanding of turbulence be embellished upon the open and eager mind of the reader. Thus, the purpose of this initial chapter seeks to review important background material critical in the understanding of the two types of turbulence, so as to make the perusal of this piece of work much easier to comprehend.

1.1 Fluid Mechanics

The million dollar question, and still quite literally so, is that of solving the ever formidable but glorious Navier-Stokes equations. This remains till today as one of the seven Millennium Prize Problems as defined by the Clay Mathematics Institute on May 24th, 2000 [Devlin, 2002]. It was only in the second half of the twentieth century that numerical computation took over from the steely resolve of our algebraic ancestors in simulating these equations with a myriad of initialized setups for both ocean and atmospheric models. However, before enjoying the luxury of modern day computational power, it would bode well to revisit the theoretical framework established by our Fluid Mechanics foreparents on whose shoulders we stand and can catapult ourselves into the study of bother homogeneous and inhomogeneous turbulence.

Of the many forms the classical momentum equations have assumed in an attempt to solve them, the one of interest in this study is that of the Boussinesq approximation.

Within this particular simplification, the density ρ is taken as constant in the momentum and continuity equations and density variations can be neglected except in the the gravity term. A general rule of thumb as to when this approximation can be implemented, as given by Kundu et al. [2012] is when:

- the Mach number of the flow is small

- propagation of sound or shock waves is not considered

- the vertical scale of the flow is not too large (as compared to scale height), and

- temperature differences in the fluid is small.

The uniformly stratified Boussinesq equations, without the effects of planetary rotation, are written as:

$$\frac{D\boldsymbol{u}}{Dt} = -\nabla p + \alpha T \hat{z} + \nu \nabla^2 \boldsymbol{u}, \tag{1.1}$$

$$\frac{DT}{Dt} + \beta w = \kappa \nabla^2 T, \tag{1.2}$$

$$\nabla \cdot \boldsymbol{u} = 0, \tag{1.3}$$

where $\boldsymbol{u} = (u, v, w)$ is the velocity, p is the perturbation pressure scaled by a reference density, and T is the potential temperature fluctuation around a linearly varying basic state. The kinematic viscosity ν and diffusivity κ are constant and related by $\kappa = \nu/Pr$, where Pr is the Prandtl number. The constants α and β are the thermal expansivity and background temperature gradient, respectively. The traditional Boussinesq equations are derived under the assumption that the density is treated as a constant except in the gravity term. This density is $\rho = \rho' - \bar{\rho}(z)$ where ρ' is the perturbation density, $\bar{\rho}(z)$ is the background density profile and $\rho' << \bar{\rho}$. Given this definition, it can be argued that the temperature fluctuations are proportional to the density fluctuations. Furthermore, in this work, β is treated as a constant. As per the assumption of the traditional Boussinesq equations, the more general case would be to allow this background temperature gradient to vary with z.

The Boussinesq equations serve as the starting point in the study of stratified turbulence in the atmosphere and oceans. At this point, a definition of turbulence would be extremely beneficial to anyone reading this but to do just that would be to stoke the flames of an already effervescent and both literally and figuratively turbulent academic community. Thus, it is best to trod on this volatile path by instead describing turbulence. After all, a

picture is worth a thousand words or even more in this case. Turbulence in fluids is an ever dynamic process where it is worthwhile to study the energy processes and the length scales over the region in which it occurs along with the values of characteristic parameters which provide insight and details as to the behaviour of the same region with time. Additionally, it may be just as beneficial to give some characteristics of turbulence to help paint a picture that will help further any such understanding. Kundu et al. [2012] gives:

- fluctuations can be irregular, chaotic and unpredictable in turbulent flows with respect to dependent field parameters like velocity and temperature,

- nonlinearity which presents itself at the end of a non-linear transition process from instability and vortex-stretching where 3D turbulence maintains its fluctuations,

- vorticity is one characteristic feature of eddies associated to their spinning nature and a variety of them exist in a range of sizes within the domain,

- dissipation occurs due to viscosity acting on the smallest eddies created from vortex-stretching transferring energy to smaller scales from the largest eddies,

- diffusivity due to the rapid mixing and diffusion of momentum and heat which stems from the prominence of agitations and overturning motions.

Understanding how the energy changes within the life cycle of a turbulent region is important in tracing what happens from large scales to small scales. The largest eddies, which are the size of the respective domain, contain the most amount of energy in the turbulent system. This occurs due to these large eddies extracting energy from the mean flow and in due process, create a strain field which affect eddies which are just smaller than them. These slightly smaller eddies then extract energy from the larger eddies in the same manner than the largest eddies extracted energy from the mean flow. This process continues for subsequent smaller and smaller eddies in which energy is cascaded down from large to small eddies by interaction with eddies of similar sizes [Kundu et al., 2012]. The word 'strain field' has been mentioned and it is worth spending some time on this term and understanding its importance in this cascade process. Through well constructed through modern research, the average cascade of energy was first proposed by Richardson [1965]. The transfer of energy from large to small eddies is driven by vortex stretching and culminates in dissipation at the Kolmogorov scale. When vorticity is exposed to a strain-rate field, it is subject to stretching. This vortex stretching involves an exchange of energy as the strain field does deformation work on the vortices being stretched. With this, the total amount of energy in the vortices is expected to increase with such an effect

3

[Tennekes and Lumley, 1972]. Thus, it can be seen that smaller eddies in the strain-rate field of a slightly larger eddy extracts energy from it and this downward cascade of energy occurs and this is called a forward cascade of energy [Tennekes and Lumley, 1972, Kundu et al., 2012]. There have been studies done on the existence of an inverse energy cascade which finds prominence in 2D turbulence [Kraichnan, 1967, Davidson, 2004, Kundu et al., 2012] but with respect to 3D turbulence, the forward energy cascade is what has been shown to dominate [Kundu et al., 2012].

From all this, calculating the values of energy throughout the life cycle of a turbulent region gives important information as to the evolution of the turbulent region. The kinetic and potential energy per unit mass can be calculated in physical space as:

$$\text{KE} = \frac{1}{2}(u^2 + v^2 + w^2), \tag{1.4}$$

$$\text{PE} = \frac{1}{2}\frac{\alpha}{\beta}T^2. \tag{1.5}$$

1.1.1 Stratified Turbulence

Characteristic of stratified turbulence are certain parameters which tell various properties of the habituated fluid. These parameters include but are not limited to the Reynolds number, Froude number, Richardson number and Prandtl number. Within this study, the Reynolds and Froude numbers are particularly considered but there are a number of studies that consider the Richardson [Smyth and Moum, 2000b, Riley and deBruynKops, 2003] and Prandtl [Smyth and Moum, 2000a, Legaspi and Waite, 2020] numbers.

The Reynolds number Re gives the ratio between the inertia and viscous forces in the fluid. A flow with low Re is characteristic of smooth laminar flow and high Re is testament to chaotic turbulent flow. The Reynolds number is defined as

$$Re = Ul/\nu, \tag{1.6}$$

where U is the characteristic flow velocity and l is the characteristic horizontal length scale of the flow. The Froude number is the ratio between inertia and buoyancy forces and the smaller this parameter, the more stratified is the fluid in questions. The Froude number is defined as

$$Fr = U/Nl, \tag{1.7}$$

where U is the fluctuation velocity, l is the characteristic length scale of this velocity and N is the Brunt-Väisälä frequency. As with the length scales, there also exists horizontal and

vertical Froude numbers Fr_h and Fr_v, defined with characteristic horizontal and vertical length scales l_h and l_v, respectively. Small horizontal Froude numbers, $Fr_h < 1$, are one of the requirements to indicate a strongly stratified regime along with the vertical Froude number being $Fr_v \sim 1$ [Waite and Bartello, 2004, Brethouwer et al., 2007]. The latter point relates an approximate balance between the inertia and buoyancy forces for stratified turbulence [Maffioli, 2017]. In achieving this value for Fr_v, the vertical length scale adjusts to the stratification in the manner of $l_v \sim U/N$. This infers that the greater the N, the smaller the l_v and this indeed affects the size of the eddies in the turbulent flow.

In Riley and Lelong [2000], two types of scalings were applied to the Navier-Stokes equations under the Boussinesq approximation and it was found that stratified turbulence possesses a non-propagating component comprising of vortical motion and a wave component based on internal wave theory. Vortical motion describes horizontal and rotational flow that does not do any work against gravity. Excitement by these eddies is one way that contributes to the generation of waves in the turbulent region. Just as the total energy is the sum of the kinetic energy and potential energy, it can also be broken down as the sum of vortex energy and wave energy, corresponding to the vortical and wave motion in a stratified flow. The vortex and wave energies can be calculated from the Craya-Herring decomposition [Kimura and Herring, 2012]. Given a wavenumber vector $\boldsymbol{k}$ and $\hat{\boldsymbol{u}}(\boldsymbol{k})$ where $\hat{\boldsymbol{u}}$ is the Fourier component of velocity such that $\boldsymbol{k} \cdot \hat{\boldsymbol{u}} = 0$, then two independent vectors can span $\hat{\boldsymbol{u}}$ in the plane perpendicular to $\boldsymbol{k}$. These two independent vectors can be broken down in one that is horizontal and vortical and the other is vertical and wavy [Kimura and Herring, 2012]. One step further gives the vortex energy as simply the horizontally rotational kinetic energy and the wave energy as the sum of the horizontally divergent kinetic energy, the potential energy and the vertical kinetic energy.

It has been mentioned above how strongly stratified turbulence is indicated by the presence of small Fr_h. It should also be mentioned how this kind of stratification physically affects the fluid. In the initial times where turbulence is rampant in a given region, the erratic and chaotic behaviour can easily be visualized with software by observing the twisting and curling patterns in the fluid. However, the stratification of a fluid comes soon into play which acts to suppress the stretching of eddies into quasi-horizontal pancake-like structures [Hebert and de Bruyn Kops, 2006, Maffioli et al., 2014, Lang and Waite, 2019]). Thus, a layering of these eddies can be seen given sufficient time where the thickness and amounts of these layers depend on the stratification of the respective fluid. The greater the stratification, the thinner these layers and vice-versa. Thus, it helps to establish the relationship between the stratification given by the buoyancy parameter N to the length scales observed in the simulated fluid. Given these length scales and velocity of the fluid, the Reynolds and Froude numbers play significant contributions in categorizing and explaining

stratified turbulence.

A salient feature of stratified turbulence is the generation and propagation of internal gravity waves. Within fluid mechanics, there are two wave speeds to be acquainted with. The first is the phase speed c which gives the speed of individual crests and troughs and the second is the group speed c_g which is the speed in which an envelope of wave packets travel [Kundu et al., 2012]. In a stratified fluid, internal waves may propagate in any direction and at any angle to the vertical. Due to this, the direction of the wavenumber becomes important and its three-dimensionality is utilised $\boldsymbol{k} = (k, l, m)$. Thus, c_g no longer refers to group speed with respect to waves in stratified fluids but rather to group velocity as it is no longer a scalar quantity [Kundu et al., 2012]. It is this c_g that is of interest when it comes to gravity waves being emanated from a stratified fluid as this is the velocity by which the wave energy propagates at some certain wavenumbers. Kundu et al. [2012] goes on to show that the wave motion which is related to the group velocity by definition is perpendicular to the wavenumber vector as well as the fact that the group velocity vector is the gradient of wave frequency ω in wavenumber space. Fortunately, in Kundu et al. [2012], the wave frequency is succinctly defined as $\omega = N cos\theta$ where θ is the angle of the wavevector $\boldsymbol{k}$ to the horizontal and can be calculated through some simple algebra. The value of the frequency is bounded by $0 \le \omega \le N$ and for waves in stratified fluids, it depends only on the direction of the wavenumber and not its magnitude. Maffioli et al. [2014] took an alternative route to this approach to prove the existence of such gravity waves by proving their experimental and simulated waves were linear. In terms of wake studies, various angles for the gravity waves were discovered given the degree of turbulence as scribed in Zhou and Diamessis [2019] and Rowe et al. [2020].

1.2   Homogeneous Stratified Turbulence

Homogeneous stratified turbulence has occupied the limelight of experimental and numerical simulations for decades and continues to be much pursued due to the sheer versatility in being able to model various initial conditions and setups. Experimental homogeneous stratified turbulence has enlightened into many characteristics of turbulence which leads on to the formation of the world renown and well-loved vortical pancake structures [Billant and Chomaz, 2000a], various power-law relationships for energy at different length scales and the generation of internal waves. These experiments are sometimes coupled with numerical simulations to compare and affirm theoretical results or act as points of reference for more modern papers to agree with results to varying degrees of accuracy. With the modern advancement in intensive computing capabilities, numerical simulations are ex-

tremely popular and entire physical setups are modelled purely numerically as in the case of towing spheres through a tunnel of stratified fluid and analysing the wakes produced.

Another prominent feature of stratified turbulence is the existence of a power-law energy spectrum for various ranges of wavenumbers. A myriad of literature is present today which illustrated the slope of these spectra given certain transitory points in the wavenumber values. Kolmogorov [1941b] established the $-5/3$ power-law relationship for isotropic unstratified turbulence in the inertial subrange where shear and viscosity do not have much effect. Even though this power-law was found in 1941, it took some more years into the twentieth century to confirm this result. In modern literature, it has been a benchmark that experimental setups and numerical runs strive to achieve this else produce reasons or considerations as to why differing values were obtained. Spectral slopes vary in stratified turbulence, which is not isotropic, and depends on whether horizontal or vertical wavenumbers are considered [Maffioli, 2017, Lang and Waite, 2019]. These slopes have critical markers that involve the buoyancy scale

$$l_b = U/N, \tag{1.8}$$

[Billant and Chomaz, 2001, Waite, 2011] where U is the velocity of the largest scale eddies and N has been defined above. The value of the buoyancy scale is also critical in stratified turbulence as it indicates the thickness of the pancake-like vortices that develop and the overturning of gravity waves [Waite and Bartello, 2004, Waite, 2011]. The greater the stratification (the bigger the N), the smaller l_b becomes and hence the pancakes become thinner. Then, there is the Ozmidov scale

$$l_O = (\epsilon/N^3)^{1/2}, \tag{1.9}$$

where ϵ is the kinetic energy dissipation rate. This scale signifies the transition from stratified turbulence to isotropic 3D turbulence [Dougherty, 1961, Ozmidov, 1965, Waite, 2011, Lang and Waite, 2019]. Below the Ozmidov scale, the eddies evolve without the influence of stratification [Brethouwer et al., 2007]. Finally, the Kolmogorov scale, also known as the dissipation scale,

$$l_d = (\nu^3/\epsilon)^{1/4}, \tag{1.10}$$

[Kolmogorov, 1941a] is where viscosity affects the fluid and dissipation of energy from small scale eddies occurs. This dissipation is defined as $\epsilon = 2\nu\langle s_{ij}s_{ij}\rangle$ where $\langle\cdot\rangle$ is the domain average and s_{ij} is the strain rate tensor [Wyngaard, 2010, Kundu et al., 2012]. Between the wavenumbers that map these length scales are defined spectral slopes that have been found in the literature which are indicative for stratified turbulence. For the horizontal spectra, $-5/3$ has been found from small wavenumbers to $k_O = 1/l_O$ and also between

k_O and $k_d = 1/l_d$ [Almalkie and de Bruyn Kops, 2012, Augier et al., 2012, Brethouwer et al., 2007, Lang and Waite, 2019]. For the vertical spectra, a steeper slope of -3 has been discovered [Maffioli, 2017]. Even though this study does not involve rotation through the Coriolis term in the Navier-Stokes equation, it is still worth mentioning that such research has found spectral slopes of $-5/3$ and -3 for divergent and rotational ranges of wavenumbers in rotating-stratified turbulence [Kitamura and Matsuda, 2006]. It has been an adventure for a vast amount of research to achieve this proportionality for various types of stratified turbulence experiments and simulations. However, a range of values can be found from -1 to $-7/3$ depending on certain conditions such as if the buoyancy Reynolds number, defined as

$$\mathcal{R} = ReFr_h^2, \tag{1.11}$$

is much greater or much lesser than 1 [Waite and Bartello, 2004, Brethouwer et al., 2007, Waite, 2011].

Given the introduction of the Reynolds and Froude numbers as well as notable wavenumbers numbers, another critical parameter for stratified turbulence is the buoyancy Reynolds number, which has already been defined in equation (1.11), but can be expressed as a ratio between the Ozmidov and Kolmogorov wavenumbers such that

$$\mathcal{R} = (k_d/k_O)^{4/3}, \tag{1.12}$$

which helps in establishing a large enough inertial range between k_O and k_d to accurately measure the small scale behaviour of turbulence [Lang and Waite, 2019]. For strongly stratified turbulence, the horizontal spectra has a slope of $-5/3$ when $\mathcal{R} \gg 1$ otherwise it becomes steeper [Brethouwer et al., 2007]. In addition to talking about the large scale behaviour of turbulence, it is equivalently worthwhile to study what happens at the smaller scales where viscous dissipation plays an important role in energy distribution. Brethouwer et al. [2007] quoted the importance of studying both Reynolds and Froude numbers in understanding stratified and strongly stratified turbulence. Various studies alluded to the importance of the value of Re whilst others extended on the understanding that small Fr_h points to a salient feature of stratified turbulence. In Smyth and Moum [2000a] and Brethouwer et al. [2007], the buoyancy Reynolds number was reintroduced and certain properties are guaranteed whether $\mathcal{R} > 1$ and $\mathcal{R} < 1$ [Brethouwer et al., 2007]. When $\mathcal{R} \gg 1$, anything with length scales at the Ozmidov length scale and greater are affected by stratification but not so for length scales much smaller than l_O; the Kolmogorov length scale l_d falls in this range. When $\mathcal{R} < 1$, viscous effects are prominent at all scales through vertical shearing activity.

Brethouwer et al. [2007] used the buoyancy Reynolds number to affirm that the $-5/3$ power law relationship holds for horizontal spectra and that the -3 power-law was found

for vertical spectra. This occurs, however, for $\mathcal{R} \gg 1$ which is the characteristic range of strongly stratified turbulence. Such a power-law is more visible with $\mathcal{R} \gg 1$ as this tells of a clear inertial range. Maffioli and Davidson [2016] ran DNS of unforced stratified turbulence and also found agreement with the $k_h^{-5/3}$ for horizontal spectra but found no such k_v^{-3} for vertical spectra. Rather, the vertical spectra found closer association with the -5/3 law. They attributed this to not having sufficiently low enough horizontal Froude number and suggested that $Fr_h \sim O(10^{-3})$ and a scaling of $Fr_v \sim 1$ would hold over a range of wavenumbers. However, they alluded to the fact that getting such low horizontal Froude numbers with $\mathcal{R} \gg 1$ is computationally expensive. Along with these computational restrictions, Waite [2011] showed that the effective grid spacing and by extension the horizontal resolution affects the reproducibility of the $k_h^{-5/3}$ spectra. With an unresolved buoyancy scale and coarse grid spacing, spectra are shallower than expected. However, if the grid spacing $\Delta x < l_b$, the spectra is steeper and in particular is k_h^{-2}. Other studies have gotten such a slope but he alludes to the fact that the way parameterizations are done for eddy viscosity and hyperviscosity are important in resolving microscale turbulence on the mesoscale. Furthermore, he stresses the need for an appropriate numerical truncation to ensure an accurate cascade of energy resulting in an appropriate power-law relationship and to not eliminate any sort of dynamics which would result in otherwise. An example of this is filtering out horizontal scales at the buoyancy scale but l_b is a critical transitory value for the forward cascade of energy for 3D turbulence.

The vertical spectrum offers quite a few differences to the horizontal one. Firstly, the vertical spectra have been found to obey a slope of -3 in Maffioli [2017]. In this paper, it was established that to achieve the slope of -3, the vertical spectra needs to be split into large scale vertical spectra and small scale vertical spectra using a horizontal demarcation scale to separate them. Moreover, this particular slope holds for $k_b \leq k_v \leq k_O$. A similar analysis was done for the potential energy spectra where the golden value of -3 was again procured but for a smaller range of wavenumbers. Furthermore, as quoted in the paper, "this evidence supports the existence of a scale-by-scale balance between inertia and buoyancy occurring in strongly stratified turbulence at large horizontal scales" [Maffioli, 2017]. Such a balance is telling in that that $Fr_v \sim 1$ is also mentioned in Billant and Chomaz [2000b,c]. Similar to how such ranges can be established, spectral slopes can transition into each other between them. Carnevale et al. [2001] quoted a slope of -3 for the buoyancy range into a $-5/3$ slope for the inertial range and this change of ranges is demarcated by the Ozmidov wavenumber. Whilst they acknowledged that a full description of the transition would require a 3D wavevector framework due to the anisotropy of the buoyancy range and isotropy of the inertial range, Carnevale et al. [2001] defined their energy sepctra with respect to a general wavenumber k. Moreover, this transition of slopes

9

between the large scale buoyancy range and the small scale inertial range occurs only for periods of active breaking. Breaking was also defined in Carnevale et al. [2001] as the process where sinusoidal waves on the most disturbed isosurface fold over to form elongated overturns leading to convectively unstable regions which then break. One point to note was that they achieved a shallower spectra of $-7/3$ but the resolution was not fantastic at 256. When this resolution was doubled, the spectral slope became shallower which would lead to a more accepted slope value from modern day literature. Another investigation into the value of the spectral slope comes in Lang and Waite [Lang and Waite, 2019] where the anisotropy of large scale directional spectra which depends on the wave vector angle. Near horizontal wavevectors have spectral slopes of -1 or shallow and near vertical wave-vectors have a slope of -3. These spectra reduce to $k_h^{-5/3}$ when vertically integrated but directional spectra have slopes of $-5/3$ at certain angles. In the interest of giving scope for such transitional behaviour, Kitamura and Matsuda [2006] found a point where the rotational component of the spectra having a value of -3 also saw a divergent component of the spectra following a $-5/3$ value. It should be duly noted that they cater for the Coriolis effect which is not done in this study but this point should just serve as an interesting fact.

Another feature of note for homogeneous turbulence in a stratified fluid is the formation of pancake-like structures. Though this was introduced in the previous sections, a detailed explanation as to this salient feature of stratified homogeneous turbulence is done here. It has been noticed with the onset of turbulence and its subsequent collapse, vortical structures called eddies fill up the entire domain whether it be an experimental or numerical setup [Herring and Métais, 1989, Waite and Bartello, 2004, Brethouwer et al., 2007, Almalkie and de Bruyn Kops, 2012]. The largest of these eddies is naturally the size of the respective domain. It has been mentioned above how these largest eddies can excite eddies of a slightly smaller size and this process repeats until the domain contained a myriad of variably sized eddies. Whilst this explanations given provide a step by step outline as to the evolutionary process of the pancakes, it remains to be seen what causes them in the first place. The creation of these pancake structures and the coining of the term as such comes from Billant and Chomaz [2000a,b,c] and their discovery of a new kind of instability called the zig-zag instability. The stratification of the experimental fluid suppresses vertical activity and hence these pancake structures are elongated in the horizontal direction. Furthermore, the degree of stratification affects how thin these pancakes can be which in turn affects how much of them can be layered in the domain. The greater the stratification, the thinner the layers and hence they are more abundant. This thickness scales with the buoyancy length scale $l_b = U/N$ [Billant and Chomaz, 2001]. Knowledge of the eddy length scales is vital information in calculating Froude numbers as strongly

stratified regions have Froude numbers $Fr_h \ll 1$ and $Fr_v \sim 1$.

Whilst homogeneous turbulence serves as an important first step in understanding this natural phenomenon, it has its limitations. One such consideration is that turbulence is not homogeneous in nature but occurs in patches in the atmosphere and oceans. This feature of turbulence is called intermittency. Global intermittent turbulence is characterized by alternating quiescence and bursting processes such as laminar and turbulent states of the atmospheric boundary layer [He and Basu, 2015] and vertical mixing of pollutants [Mahrt, 1989]. Whilst statistical methods have been used to average the patches of turbulence, it is of merit to study such systems on a somewhat individual basis. Thus, it is of interest to study how these turbulent patches singly interact with a non-turbulent environment.

1.3   Inhomogeneous Stratified Turbulence

Homogeneous stratified turbulence, whether in the ocean or atmosphere, has been and still currently is an ever exciting, effervescent field of study. There are many such experiments and simulations done which considers forcing, stratification or any combination of those features. While simulating various initializations of homogeneous turbulence give results which are quite indicative and telling in its behaviour in nature given certain conditions, one key characteristic is not accounted for. This is the global or external intermittency that turbulence possesses. This essentially tells that turbulence occurs in patches or clouds which can see the organization of such structures on scales larger than the main eddies [Mahrt, 1989] and involves due consideration of the behaviour of the boundary between the turbulent and non-turbulent regions [He and Basu, 2015]. The statistical uniformity that homogeneous turbulence offers does not entirely capture this fact of global or external intermittency in nature. This definition of intermittency is not to be confused with the small-scale, microscale, internal or intrinsic definition of the same term which relates to the statistics of higher-order structure functions, the dissipation of turbulent kinetic energy to mainly the small sub-regions of individual eddies [Mahrt, 1989] or a focused space/time study of the small-scale structure within turbulent flows [He and Basu, 2015]. Thus, understanding how these turbulent patches interact with their surroundings, which are either not as turbulent or not turbulent at all, is important in understanding the natural process of turbulence. Such an existence can be defined as inhomogeneous turbulence and particularly for this study, a turbulent patch is numerically analysed in its evolution in an otherwise quiescent domain.

Motivation for the initial research into inhomogeneous stratified turbulence has been presented in Riley and Metcalfe [1987] which sought to simulate a stratified horizontal cloud

with three different Froude numbers in an otherwise quiescent domain. A first point to note is that they focused their efforts entirely on inhomogeneous turbulence but in this thesis, a comparison is also made to homogeneous turbulence of a similarly sized domain. A second point to note is the size of the cloud used in the respective simulations. What should be considered is that the horizontal cloud in Riley and Metcalfe (their Figure 1) was defined to extend infinitely in the $x-$ and $y-$ directions but was localized in the z- or vertical direction. Their cloud was also initialized to be statistically homogeneous in the horizontal with a quiescent and stably-stratified background. A similar experimental setup was used for all simulations in this thesis with the primary difference being in the approaches used. Though the simulation resolution at that time was 64^3, encouraging results using Fourier transforms (through the use of a pseudo-spectral spatial method with an Adams-Bashforth time-stepping scheme) were produced which showed the evolution of kinetic, potential, wave and vortex energies in and out of the variously stratified clouds. One particular result from this paper shows that the vortex energy primarily remains within the cloud for all simulations ran with three different Froude numbers but a significant amount of wave energy was found in the initially quiet regions. Several results were presented in the paper which all attributed the presence of such wave energy to the generation and propagation of internal waves due to the effects of stratification on the turbulent cloud. Furthermore, the stronger the stratification, the greater the vertical spread of wave energy outside the cloud. This also coincided with a greater decrease in vortex energy inside the cloud. Even though this decrease was small in magnitude and the majority of the vortex energy remained localized within the cloud, it was believed that this behaviour was partly related to the subsequent wave radiation [Riley and Metcalfe, 1987]. Thus, it can be seen that the physical interaction between a turbulent patch and a non-turbulent one is able to induce internal waves in the latter.

Maffioli et al. [2014] also investigated this interaction between a stratified turbulent cloud and its non-turbulent surroundings to understand the formation of pancake-like vortices in the latter region. Before going any further, it is important to note that the cloud was oriented vertically in Maffioli et al. [2014] as opposed to horizontally in Riley and Metcalfe [1987] but the mechanism of different interacting regions resulting in the generation and propagation of internal gravity waves was also present. Maffioli et al. [2014] proceeded to understand these pancake vortices both experimentally and numerically. In their experimental setup, they used a tank in which the turbulent region was put on one side and was then allowed to evolve horizontally towards the other side of the tank. They performed various pairs of such experiments with pearlessence flakes and fluorescein (green dye). The former tracks the initial movement of fluid in the turbulent cloud and internal wave presence in the non-turbulent region adjacent to the turbulent one and the

latter indicates the cloud edge deformation due to turbulent advection. By considering the position of these trackers from each other, a lot of information can be initially gained. The pearlessence flakes were found ahead of the dye and can represent different scenarios. Horizontally elongated structures as shown by the pearlessence hint to the activity of internal waves outside of the cloud whereas the displacement of the dye points towards the deformation of the cloud's edge due to turbulent advection of the fluid. To further clarify between these two situations, the numerical simulation is used to quantify these initial qualitative results. Numerically, Lagrangian particles are dispersed throughout the turbulent cloud and its position with respect to the pancake vortices is scrutinized. The edges of the pancake vortices were well ahead of the Lagrangian particles which tells that internal waves are the reason for such vortices and not advection the turbulent cloud. A further important results emanating from this paper is that these waves are linear in nature by an investigation of the group speed of these pancake vortices.

Another popular research area of inhomogeneous turbulence is the evolution of wakes from moving bodies being towed through a stratified fluid embedded in an otherwise quiescent environment [Abdilghanie and Diamessis, 2013, Zhou and Diamessis, 2019, Rowe et al., 2020]. An immediate comparison of this setup to the one in Riley and Metcalfe [1987] tells: (a) the removal of the moving body leaves the stratified fluid as an example of a turbulent cloud in an otherwise quiescent region, (b) wakes are highly turbulent and can evolve as far as secondary collapsing under stratification which doesn't happen for a freely decaying cloud, (c) Froude number calculations vary because the length scale used either considers the size of the eddies or the diameter of the moving body, (d) wakes have been calculated to follow the power-law spectra under stratification but no such analysis was done for the other paper, and (e) wakes are localized formations whereas the cloud's evolution affected the entire domain. Naturally, a significant amount of detail is emphasized on the sustainability and collapsing of these wakes as well as the creation of secondary wakes. In addition to these pivotal points, one major facet of interest is the range of angles by which internal waves are propagated into these quiescent regions. These angles are studied in depth in Abdilghanie and Diamessis [2013], Rowe et al. [2020] but not in Riley and Metcalfe [1987]. It has been found that these angles vary based on the structure of the stratified fluid due to its turbulent life cycle which lends to a correlation between the range of these angles and particular time intervals in which they occur. It has been found that a range of $20° - 70°$ [Rowe et al., 2020] can be observed for the non-equilibrium regime and it is at the end of this regime where the internal waves become fully horizontal (parallel to the orientation of the cloud and the direction of growth/spread of the pancake vortices). Depending on the experimental setup, other ranges for this wave propagation have been found as $40° - 55°$ in Abdilghanie and Diamessis [2013] and $35° - 45°$ in Dohan

and Sutherland [2003].

1.4 Thesis Objectives

Given the elaboration on both homogeneous and inhomogeneous stratified turbulence, the motivation for this research is as follows:

1. To compare the evolution of homogeneous and inhomogeneous stratified turbulence in a purely numerical setting,

2. To investigate and relate parameters such as Froude numbers, length scales, dissipation and buoyancy Reynolds numbers of inhomogeneous turbulence to those already well defined for homogeneous turbulence in the academic literature,

3. To analyse the power-law spectra of the turbulent cloud to that established in the literature for horizontal and vertical wavenumbers in homogeneous turbulence,

4. To study the generation of internal gravity waves emitted from the stratified turbulent cloud and to what angles do these waves propagate at.

Following this chapter, the numerical scheme and simulation framework is discussed in Chapter 2, results and their respective discussions are presented in Chapter 3 and a summary with perspective for future work concludes this thesis in Chapter 4.

Chapter 2

Methodology

2.1 Numerical Setup

The numerical model employed invokes the application of a spectral transform method [Durran, 2010] on a triply periodic domain of size $L_x \times L_y \times L_z$ to solve the uniformly stratified Boussinesq equations (1.1)-(1.3). This domain is broken up into $n_x \times n_y \times n_z$ grid points in physical space and an equivalent number of discrete wavenumbers in Fourier space. This gives a grid spacing of $\Delta x = L_x/n_x$, $\Delta y = L_y/n_y$ and $\Delta z = L_z/n_z$. With the use of a spectral method, the range of wavenumbers to be considered can be as follows

$$k_i = \frac{2\pi}{L_i}j, \quad j = -K_i + 1, ..., K_i, \tag{2.1}$$

where $i \in \{x, y, z\}$ and $K_i = n_i/2 \in \mathbb{Z}$ is the natural choice for dimensionless truncation wavenumber and in this study, n_i is even.

The equations are numerically computed using the third-order Adams-Bashforth method with the viscous/diffusion terms treated with a Crank-Nicolson approach [Durran, 2010]. To understand the approach, consider an equation for a given Fourier coefficient ψ

$$\frac{d\psi}{dt} = F(\psi) - r\psi, \tag{2.2}$$

where r is the viscous/damping rate and F is the total of the nonlinear and linear terms as in (1.1)-(1.3). With this, the overall Adams-Bashforth and Crank-Nicolson scheme is

$$\frac{\psi^{(n+1)} - \psi^{(n)}}{\Delta t} = \frac{1}{12}\left[23F(\psi^{(n)}) - 16F(\psi^{(n-1)}) + 5F(\psi^{(n-2)})\right] - r\frac{\psi^{(n+1)} + \psi^{(n)}}{2}, \tag{2.3}$$

where $\psi^{(n)}$ is the value of ψ at $t = t_0 + n\Delta t$. The value of ψ at time $n + 1$ depends on the previous three time steps as

$$\psi^{(n+1)} = \left(\frac{1 - r/2}{1 + r/2}\right)\psi^{(n)} + \frac{\Delta t}{12(1 + r/2)}\left(23F(\psi^{(n)}) - 16F(\psi^{(n-1)}) + 5F(\psi^{(n-2)})\right). \quad (2.4)$$

where the first and second time steps are calculated by a Runge-Kutta method. This scheme offers impressive stability properties [Durran, 2010] such that once Δt is sufficiently small to ensure the stability of the linear and advective terms then the viscous/diffusion terms will also be stable. In terms of spatial discretization, the Fourier transform is used and is explained later in this section. Furthermore, the code solves the vorticity formulation of (1.1):

$$\frac{\partial \boldsymbol{\omega}}{\partial t} = \nabla \times (\mathbf{u} \times \boldsymbol{\omega}) + \alpha \begin{bmatrix} \partial T/\partial y \\ -\partial T/\partial x \\ 0 \end{bmatrix} + \nu \nabla^2 \boldsymbol{\omega}, \quad (2.5)$$

where $\boldsymbol{\omega} = \nabla \times \mathbf{u}$ and the term in the brackets relates to the baroclinic generation of vorticity. Using incompressibility, inverting the vorticity gives the velocity by solving

$$\nabla^2 \mathbf{u} = -\nabla \times \boldsymbol{\omega}, \quad (2.6)$$

which can be be written in Fourier space as

$$k^2 \hat{\boldsymbol{u}} = i\boldsymbol{k} \times \hat{\boldsymbol{\omega}}, \quad (2.7)$$

where $\hat{\boldsymbol{u}}$ and $\hat{\boldsymbol{\omega}}$ are the Fourier transformed velocity and vorticity respectively. Equation (2.7) can easily be solved for $\hat{\boldsymbol{u}}$ by dividing through with k^2.

The spectral transform method uses a Fast Fourier Transform (FFT) to move between the physical and Fourier domains. This is advantageous as it allows model variables to be calculated in either domain wherever the numerical process is simply easier and less computationally expensive. An example of this is that quadratic non-linearities are easiest to calculate in the physical domain but derivatives are best computed in the Fourier domain. Given this advantage of the FFT connecting physical and Fourier spaces, energy calculations which are an important consideration in turbulent studies can be calculated in either domain. For example, kinetic energy can be calculated in the physical space by $1/2|\mathbf{u}|^2$ but the vortex energy is evaluated in the Fourier space by using the Craya-Herring decomposition [Kimura and Herring, 2012]. Whichever the space, the amount of energy is the same as guaranteed by Parseval's Theorem and with such a robust equivalence, the FFT is used in this model.

Given that some calculations are better carried out in physical space such as pointwise multiplication to compute non-linear terms, one unwelcome situation that can arise is that of aliasing. Aliasing can arise in the situation of pointwise multiplication of two fields where the result is of a smaller scale than the available grid spacing and it becomes unresolvable. This can then lead to numerical instabilities and cause numerical simulations to blow up. Thus, it is important that aliasing is minimized or eliminated by truncating the range of the Fourier coefficients. The truncation provided by $K_i = n_i/2$ does not effectively deal with aliasing and an alternative must be sought. In Durran [2010], truncating the wavenumbers at $n_i/3$ and rounding down to the nearest integer removes all problems associated with aliasing but some DNS simulations [Riley and deBruynKops, 2003] have truncated as far as $15n_i/32$ which was capable of removing the dominant aliasing error. For the simulations conducted in this work, the truncation is such that the maximum wavenumbers are $K_x = 4n_x/9$, $K_y = 4n_y/9$ and $K_z = 4n_z/9$ where n_x, n_y and n_z are the number of grid points in the respective Cartesian directions [Lang and Waite, 2019, Legaspi, 2019]. Such a truncation allows in getting more resolution out of the grid whilst also eliminating most aliasing. Given this range of $8n/9$ wavenumbers, the effective grid resolution for the simulations are

$$\Delta x = 9L/8n, \tag{2.8}$$

where L is the length of one side of the 2π cube.

2.2 Simulation Framework

The simulations were carried out in a cube of length $L_x = L_y = L_z = 2\pi$ that was divided into $n_x = n_y = n_z = 1024$ grid points. The majority of this study seeks to compare simulations where the entire 2π box is filled with homogeneous turbulence versus an inhomogeneous setup. The latter is a turbulent cloud being present in the middle of the domain initially occupying one-quarter of the total space for $3\pi/4 \leq z \leq 5\pi/4$ for all x and y in an otherwise quiescent box of the same size as in the homogeneous setup. The cloud was created by extracting an appropriate sized block by applying a window function on a snapshot from a homogeneous simulation to mimic a patch of turbulence with quiet regions above and below it. The inhomogeneous setup can be visualized in figure 2.1 with vorticity being greatest within the cloud and approximately zero elsewhere.

The window function used is

$$\frac{1}{2}\left[\tanh((z - z_u)/z_w) - \tanh((z - z_l)/z_w)\right], \tag{2.9}$$

where $z_u = 3L_z/8$ is the upper boundary of the cloud, $z_l = 5L_z/8$ is the lower boundary of the cloud and $z_w = \pi/10 = L_z/20$ is the thickness of the transition from within the cloud to outside the cloud as tanh goes from 1 to -1. This is shown in figure 2.1 which also includes a transect of the vorticity through fixed x and y for all z so as to distinguish activity within the cloud with the lack thereof outside of the cloud at initial time. The orientation of the cloud is parallel to the xy-plane as in Riley and Metcalfe [1987] but with much higher resolution and in Zhou and Diamessis [2019] which studies wake turbulence of a moving body in a horizontally stratified cloud. A variation to this where the the cloud was perpendicular to the xy-plane can be seen in Maffioli et al. [2014].
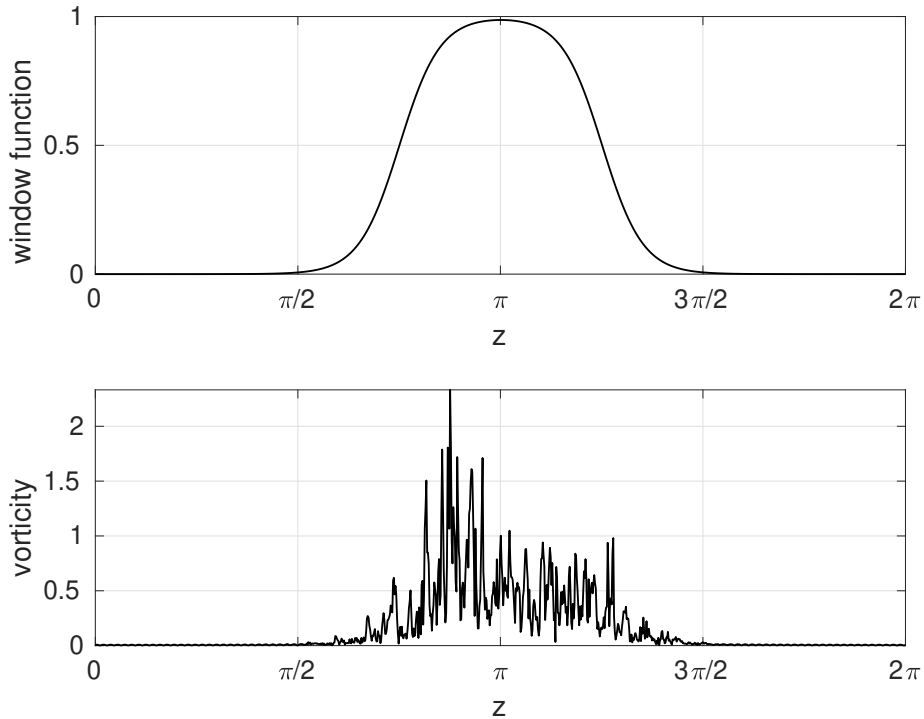
Figure 2.1: (a) The shape of the tanh window function used to create a turbulent cloud and (b) a profile of the magnitude of vorticity at fixed x and y for all z taken from the middle of the domain to help visualize the turbulent and quiescent regions at $t = 0$.

The homogeneous simulation was initialized by data from a forced unstratified turbulence simulation, which was run until statistical stationarity (energy input via forcing is equal to energy output by dissipation) was achieved [Lang and Waite, 2019]. After this, the tanh window in equation (2.9) shown by figure 2.1 was applied to this simulation of statistical stationarity which is at $t = 0$. Then, different degrees of stratification were

18

utilized, and the simulation was subsequently run without any forcing for 250 time units where the turbulence was freely decaying. The inhomogeneous setup was initialized and exposed to same levels of stratification for 250 time units. The kinematic viscosity with its respective numerical units used in the model is $\nu = 0.027 \times 10^{-4}$. This value was chosen to be as small as possible whilst respecting the resolution required for DNS. In Table 1 of [Lang and Waite, 2019], the ratio of k_{max} to k_d is less than one for their $n = 1024$ runs and the simulations in this thesis is initialized in the same manner as theirs. With the evolution of time, ϵ decreases and the resolution of the Kolgomorov scale gets better. If an inappropriate ν is chosen such that the Kolgomorov wavenumber $k_d \gg k_{max}$, the turbulence causes an unwanted accumulation of energy near k_{max} to create the necessary dissipation. This creates grid-scale noise and can more often than not lead to numerical instability. However, actual turbulence in nature transfers energy past k_{max} and is dissipated at k_d which means that k_{max} needs to be greater than k_d. Thus, ν is picked so that dissipation scale is accurately resolved which also satisfies the requirement for DNS [Pope, 2000]. Also, for this setup, $\kappa = \nu$ so that the Prandtl number is 1. The stratifications utilized are $N = 0, 0.15, 0.3$ and 0.6. These values of N indicate strong stratification as they give horizontal Froude values of $O(10^{-2})$ [Lang and Waite, 2019].

In addition to these choices of N, one more simulation is studied for $N = 0.3$ but the initialization of the simulation is forced stratified turbulence with $N = 0.3$. This particular simulation and its results will be labelled as $N = 0.3(\text{SIC})$ where SIC is an abbreviation for 'stratified initial condition'. This run is different from the other four previously mentioned because it only adjusts to the presence of the cloud whereas the others adjusts to different stratifications as well as the cloud at $t = 0$. Other important parameters are quoted in Table 2.1 for the initial time of the simulations and Table 2.2 records their values at the final time for the same simulations.

The characteristic length scale of the dominant turbulent eddies have been calculated in two ways in the literature. In Lindborg [2006] and Brethouwer et al. [2007], the formula used to calculate the vertical length scale is

$$l_v = \frac{\int_0^{k_{v,max}} E(k_v) dk_v}{\int_0^{k_{v,max}} k_v E(k_v) dk_v}, \tag{2.10}$$

whereas in Zhou and Diamessis [2019], the vertical length scale is

$$l_v = \frac{\int_0^{k_{v,max}} 2\pi k_v^{-1} E(k_v) dk_v}{\int_0^{k_{v,max}} E(k_v) dk_v}. \tag{2.11}$$

The 2π is just a scalar term in the second equation and any concern need not be placed on that. What is of interest is the choice of two different ways to calculate the vertical length scale depending on the placement of the k_v term. The argument put forward in Appendix B of Brethouwer et al. [2007] is that having k_v to the first power requires $E(k_v)$ to fall off faster that k_v^{-2} for large $k_v l_v$. To satisfy this condition is to ensure that the spectrum falls of as k_v^{-3} which is expected for stratified turbulence. They also argued that choosing k_v^2 puts too much emphasis on small scales which adds an extra dependency on the Reynolds number. However, with the approach of Zhou and Diamessis [2019], the aforementioned restrictions on the required steepness of the spectra are not needed as their approach allows for shallower spectra. This makes the second equation more robust as varying power-law relationships have been found in previous studies. Further, it avoids completely having to ensure convergence with an $k_v E(k_v)$ term in the denominator. Given the details on calculating l_v, the horizontal length scale l_h can also be calculated from the above equation (2.11) by using k_h and $E(k_h)$ where the vertical counterparts are present. Finally, the eddy time-scale τ can be computed by $\tau = l_h/U$ where U is the fluctuation velocity (discussed below). The values of these length and time scales can seen in tables 2.1 and 2.2. From table 2.1, $\tau \approx 70$ so the simulation length of 250 time units is a few eddy times scales long, which is approximately 3.6 in number.

A critical result of these simulations is the production and subsequent analysis of both horizontal and vertical spectra for the turbulent cloud. These spectra are calculated with respect to the horizontal wavenumber

$$k_h = \sqrt{k_x^2 + k_y^2}, \tag{2.12}$$

and vertical wavenumber

$$k_v = |k_z|. \tag{2.13}$$

Following Zhou and Diamessis [2019] in their calculation of the Froude number, the velocity required is the fluctuation velocity $\mathcal{U}$ within the cloud which is

$$\mathcal{U}_i = \sqrt{u_i^2 - \bar{u}_i^2}, \tag{2.14}$$

for $i \in [1, 2, 3]$ where $(u_1, u_2, u_3) = (u, v, w)$ and $\bar{u}_i$ is the average of the respective velocity component for the cloud region. It is this $\mathcal{U}$ that is used to calculate the Froude number from equation (1.7). Then, as the domain is triply periodic, it means the boundaries in the x- and y-directions are still periodic due to the orientation of the cloud with respect to the domain but not so for the z-direction. This poses a problem as the Fourier transform to produce the vertical spectra requires periodic boundary conditions to be present at the top

and bottom of the cloud. To achieve this, a Hanning window is used to achieve periodicity in the z-direction. After getting the fluctuation velocities and triply periodic boundary conditions for the shape of the cloud, a two-dimensional Discrete Fourier Transform (2D FFT) is used for obtaining the horizontal spectra and similarly, a one-dimensional Discrete Fourier Transform (1D FFT) is done for the vertical spectra. In particular, k_h may not always be an integer so it is rounded appropriately to produce such whole values. The Fourier transformed velocities are then used to calculate the different types of energy present in the cloud. The energy is then sorted according to their corresponding wavenumbers and spectra are thus established.

Due to the aforementioned ease of certain evaluations using the FFT and invoking Parseval's Theorem guaranteeing the equivalence of energy between the physical and Fourier spaces, the energy quantities to be calculated using the wavenumber spectra are kinetic (KE), potential (PE), vortex (VE) and wave energies (WE):

$$\text{KE} = \frac{1}{n_z} \sum_{h_z} \sum_{k_h} \frac{1}{2}(|\hat{u}|^2 + |\hat{v}|^2 + |\hat{w}|^2), \tag{2.15}$$

$$\text{PE} = \frac{1}{n_z} \sum_{h_z} \sum_{k_h} \frac{1}{2}\frac{\alpha}{\beta}|\hat{T}|^2, \tag{2.16}$$

$$\text{VE} = \frac{1}{n_z} \sum_{h_z} \sum_{k_h} \frac{1}{2}\frac{|ik_x\hat{v} - ik_y\hat{u}|^2}{k_h^2}, \tag{2.17}$$

$$\text{WE} = \frac{1}{n_z} \sum_{h_z} \sum_{k_h} \frac{1}{2}\frac{|ik_x\hat{u} + ik_y\hat{v}|^2}{k_h^2} + \text{PE} + \text{KE}_z. \tag{2.18}$$

where h_z is the vertical grid level index. The Fourier transform performed for the above energy calculations is in x and y only so that $\hat{u}(k_x, k_y, z, t)$, $\hat{v}(k_x, k_y, z, t)$ and $\hat{w}(k_x, k_y, z, t)$. Also, in calculating the potential energy, it should be emphasized from equations (1.1)-(1.3) that β is constant.

The final parameter of interest in this study is the eddy frequency ω_e at horizontal wavenumber k_h defined as

$$\omega_e(k_h) = \sqrt{k_h^3 E(k_h)}. \tag{2.19}$$

The derivation of the above equation (2.19) centres around 'an eddy of scale r' which possesses a scale approximately between $r/2$ and $3r/2$ so that about scale r, it lies in a band of width $\Delta r \sim r$ [Tennekes and Lumley, 1972, Wyngaard, 2010]. Using the eddy of scale r, the corresponding wavenumber magnitude can be written as $k \sim 1/r$ and the

velocity scale $u(r)$ has a relationship such that

$$[u(r)]^2 \sim kE(k), \tag{2.20}$$

where $E(k)$ is energy at wavenumber k [Wyngaard, 2010]. Thus, taking the square root on both sides of equation (2.20) and multiplying across by k gives the eddy frequency as in equation (2.19). As discussed in the previous chapter, the action of eddies are important in the excitement of internal waves [Riley and Metcalfe, 1987, Maffioli et al., 2014]. What also is known is that the dominant eddies which are also the largest eddies possess the most energy in the domain. Thus, it is expected that frequency of waves which are generated and propagated for varying N to be close to the eddy frequency of these dominant eddies. From $\omega_e(k_h)$, the angle of propagation of these waves can be calculated by assuming that ω_e is similar to the wave frequency $\omega = N\cos(\theta)$ where θ is the angle that the wavevectors make with the horizontal.

The output files produced from the simulations underwent post-processing in Matlab and Paraview in an effort to understand the non-forced, decaying behaviour of the homogeneous and inhomogeneous simulations through graphical plots and pictorial representations. These two pieces of software granted many advantages in that the FFT and inverse FFT are easily calculated via Matlab and a visual representation of the collapsing of turbulence, the layering of the pancake vortices, extensions of the cloud and propagation of gravity waves was captured by Paraview. The code used for generating the NetCDF files were scripted in Fortran, which utilized 512 cores, taking approximately 20 hours to run. The post-processing of the NetCDF files were done in Matlab which using 12 CPUs for a approximate completion time of 18 hours. Both the simulations and post-processing were all performed on Compute Canada's Graham clusters.

N	τ	ϵ	l_v	l_h	Fr_v	Fr_h	Re_b	k_b
0	70.4	0.191×10^{-5}	2.49	1.23	-	-	-	-
0.15	70.4	0.191×10^{-5}	2.49	1.23	0.0470	0.0947	31.4	8.57
0.30	70.4	0.191×10^{-5}	2.49	1.23	0.0235	0.0473	7.85	17.1
0.60	70.4	0.191×10^{-5}	2.49	1.23	0.0117	0.0237	1.96	34.3
0.30(SIC)	88.1	0.123×10^{-5}	2.41	1.84	0.0290	0.0378	5.07	14.3

Table 2.1: Values of parameters at the beginning of the inhomogeneous simulations within the cloud.

N	τ	ϵ	l_v	l_h	Fr_v	Fr_h	Re_b	k_b
0	248	9.25×10^{-8}	2.12	1.30	-	-	-	-
0.15	232	7.57×10^{-8}	2.60	2.24	0.0248	0.0288	1.25	15.5
0.30	204	1.03×10^{-7}	2.45	2.26	0.0151	0.0163	0.423	27.1
0.60	185	1.20×10^{-7}	2.43	2.21	0.0082	0.0090	0.124	50.4
0.30(SIC)	207	1.67×10^{-7}	2.04	2.54	0.0200	0.0161	0.688	24.4

Table 2.2: Values of parameters at the end of the inhomogeneous simulations within the cloud.

Chapter 3

Results

This chapter seeks to compile results from the various simulations so as to accurately comment on the comparison between homogeneous and inhomogeneous turbulence. In particular, the behaviour within the cloud is contrasted with that outside of the cloud and then referenced to the homogeneous turbulence simulations where there is no such distinction. Outside of the cloud here is defined in this section as $z < L_z/4$ and $z > 3L_z/4$ which is a more restricted region to what was defined in Chapter 2. These regions within the domain can be seen in figure 3.1. The evolution of the turbulent cloud imbibes certain dynamics into the regions immediately above and below it in which the boundary separating the cloud from the rest of the domain becomes quite unclear. The influence of the cloud thus extends beyond the initially defined boundaries through processes such as molecular diffusion and advection so that to get an accurate representation for the out of cloud behaviour, calculations are done for the upper and lower quarters of the cubic domain.

The sections in the chapter account for various parameters such as horizontal length and vertical length scales, horizontal and vertical Froude numbers and buoyancy Reynolds numbers. In addition to such parameters, a variety of diagnostics is also presented such as time series for energy, rates of dissipation, possible angles of propagation for internal gravity waves, and energy spectra at given times. Both these parameters and diagnostics will be compared to other works done on turbulence to see how they relate to each other. Within each of these sections, a discussion is also offered so as to aid the reader in their journey of this comparative and exploratory research effort. For this chapter, UIC refers to unstratified initial condition and SIC refers to stratified initial condition.
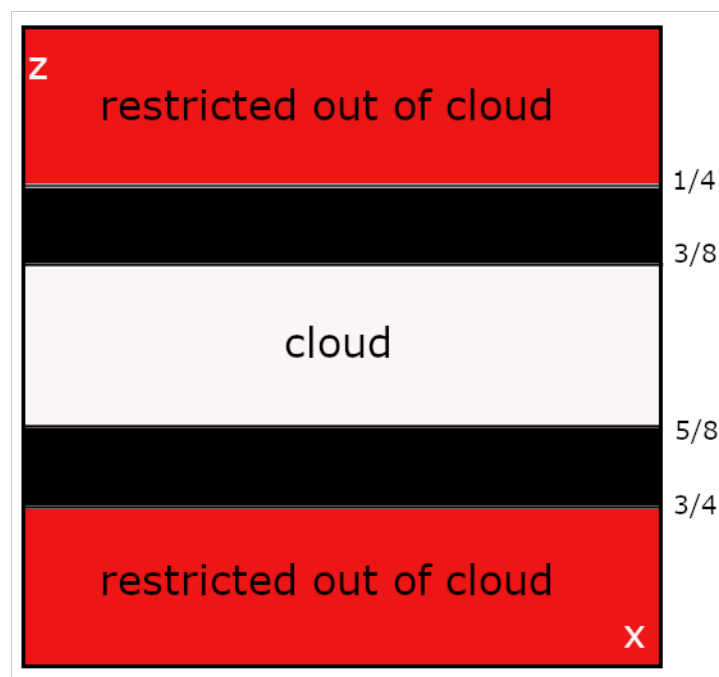
Figure 3.1: A vertical $(x - z)$ slice of the domain showing the cloud and restricted out of cloud regions.

3.1 Energy Time Series

3.1.1 Kinetic Energy

Figure 3.2: Time series of kinetic energy averaged over the defined cloud region for (a) $N = 0$, (c) $N = 0.15$, (e) $N = 0.3$, (g) $N = 0.6$, (i) $N = 0.3$(SIC) and outside the cloud region for (b) $N = 0$, (d) $N = 0.15$, (f) $N = 0.3$, (h) $N = 0.6$, (j) $N = 0.3$(SIC).

Figure 3.2 compares the evolution of kinetic energy inside the cloud (plots on the left) and outside the cloud (plots on the right), both normalized by the initial total energy inside the cloud for the homogeneous and inhomogeneous systems. Within the cloud, it can be noticed that the decay of the kinetic energy is similar for both system with the inhomogeneous system decaying slightly faster. This is most noticeable for the more stratified cases with $N = 0.3$ and $N = 0.6$ within the first half of the time allotted for the simulation. However, a stark contrast comes out of the cloud with respect to the inhomogeneous run in which there is an overall increase in the amount of kinetic energy which can be observed. It should be pointed out that this energy is quite small for $N = 0$

but it does increase as N get larger. This is seen for panels (d)-(h). An explanation for this, which appears to be accurate and is discussed further in this chapter, is that the turbulence in the cloud excites waves which propagate out of the cloud. The SIC case in panels (i) and (j) has a continuous decrease in kinetic energy within the cloud as compared to the almost horizontal plateau achieved by the UIC cases for later times $t > 100$. The energy outside of the cloud for the SIC case does increase with time but is also a magnitude of $O(10)$ smaller than that for the UIC cases with $N \neq 0$. It seems that the adjustment to stratification plays a role in the out of cloud behaviour when comparing the UIC and SIC cases. Again, the adjustment to stratification plays in role in the UIC and SIC cases for $N = 0.3$.
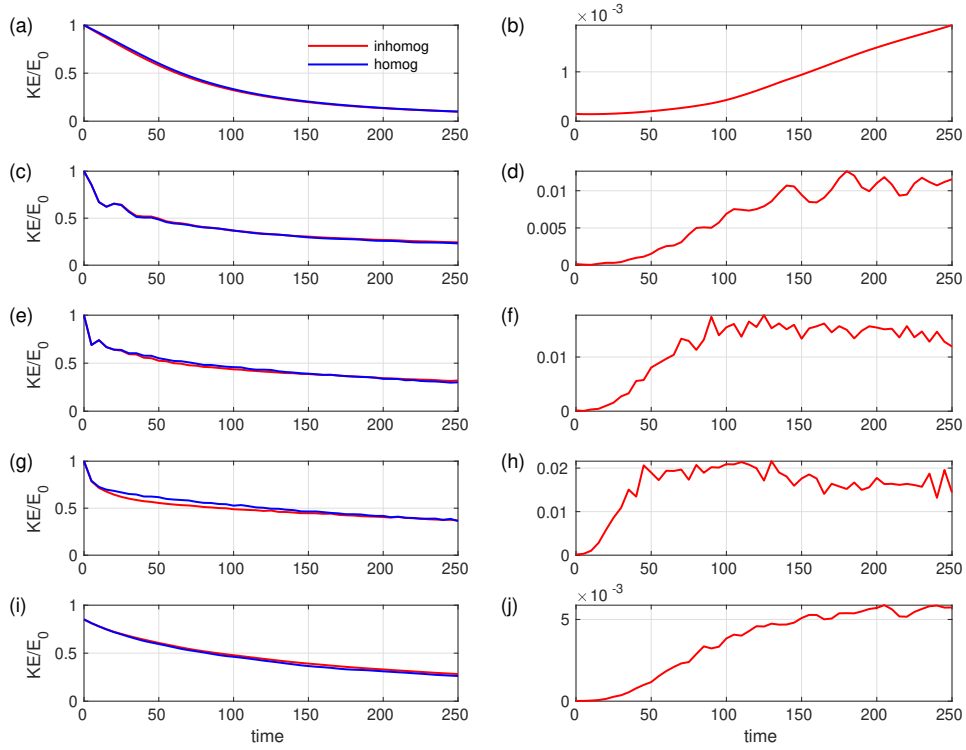
3.1.2 Potential Energy
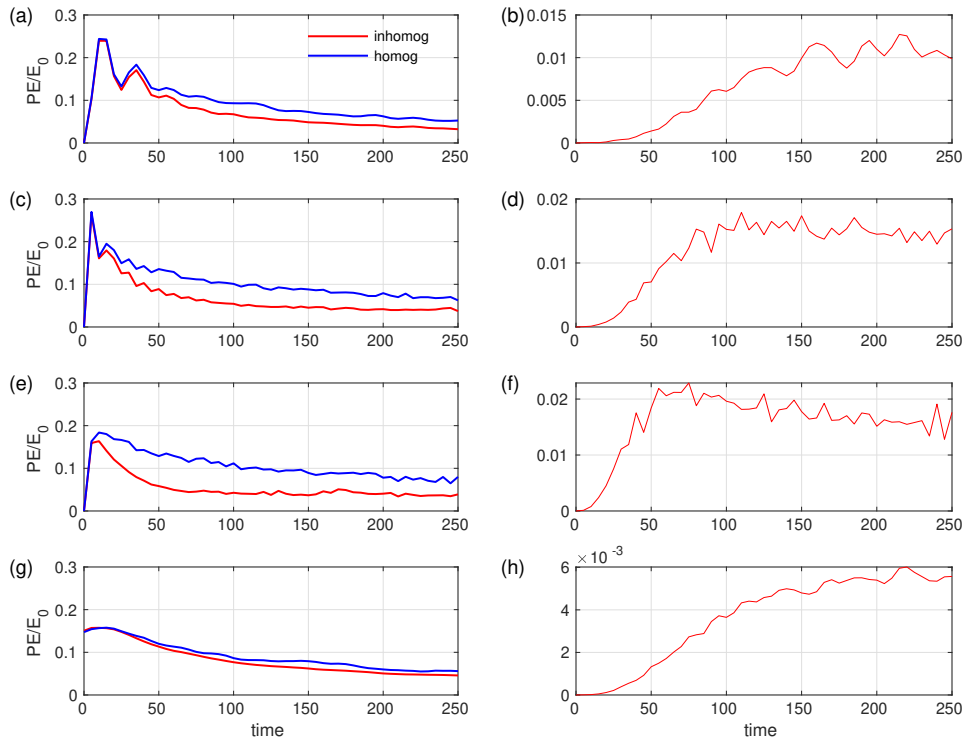

Figure 3.3: Time series of potential energy averaged over the defined cloud region for (a) $N = 0.15$, (c) $N = 0.3$, (e) $N = 0.6$, (g) $N = 0.3$(SIC) and outside the cloud region for (b) $N = 0.15$, (d) $N = 0.3$, (f) $N = 0.6$, (h) $N = 0.3$(SIC).

Figure 3.3 compares the evolution of potential energy inside the cloud (plots on the left) and outside the cloud (plots on the right), both normalized by the initial total energy inside the cloud for the homogeneous and inhomogeneous systems. The plots show that the potential energy decays more rapidly for an increasing N in the UIC cases. Due to the presence of stratification and increasing the strength thereof, this reduction of potential energy within the turbulent cloud suggests that there is an increase in internal waves being propagated into the region outside of the cloud. This point is reinforced by the increase in potential energy outside of the cloud. Consider a reference energy value of 0.02 for panels (b) $N = 0.15$, (d) $N = 0.3$ and (f) $N = 0.6$ on the right hand side. The potential energy outside the cloud: is less than half of the reference value for (b), is slightly smaller than the reference value for (d) and is greater than the reference value for (f). Thus, the potential energy outside of the cloud increases as N get larger. Another check for this is to observe the wave energy outside of the cloud (Figure 3.5). It is also worth noting that the inhomogeneous systems inside the cloud depicted in panels (a), (c) and (e) on the left hand side all decay to an energy value of approximately 0.05 which is about half the value of the homogeneous systems for the same region at the end of the simulations. The SIC case in panels (g) and (h), however, offers different results in that the potential energy in the cloud for both systems decay to an approximate value of 0.05 with the inhomogeneous system decaying faster. Also, there is an increase of potential energy outside of the cloud as shown in panel (h) but is a magnitude of $O(10)$ smaller as compared to the UIC cases outside of the cloud.

3.1.3 Vortex Energy

Figure 3.4 shows the vortex energy inside the cloud (plots on the left) and outside the cloud (plots on the right), both normalized by the initial total energy inside the cloud for the homogeneous and inhomogeneous systems. It can be seen within the cloud that the inhomogeneous system experiences an extremely similar evolution to that of the homogeneous system as shown by the almost perfect overlap of the curves. As can be seen with greater N, the vortex energy does not decay much with time similar to Riley and Metcalfe [1987] in that vorticity is localized to the turbulent cloud and does not spread out as easily to the non-turbulent areas. It can also be noticed that the vortex energy outside of the cloud is somewhat constant from the horizontal slope of the curves with some oscillatory behaviour also being present which is particularly displayed in panel (d). This can be related to waves outside of the cloud. Linear waves do not possess any vortex energy but due to nonlinearities, there will be a small amount of vortex energy in the waves. This can also be the case for panels (f) and (g) but there was not a high enough output frequency to

Figure 3.4: Time series of vortex energy averaged over the defined cloud region for (a) $N = 0$, (c) $N = 0.15$, (e) $N = 0.3$, (g) $N = 0.6$, (i) $N = 0.3$(SIC) and outside the cloud region for (b) $N = 0$, (d) $N = 0.15$, (f) $N = 0.3$, (h) $N = 0.6$, (j) $N = 0.3$(SIC).

resolve. The minuscule energy value of these curves reiterate the fact that the vast amount of vortex energy remains localized in the turbulent cloud. This slight increase of energy outside the cloud can be attributed to the evolution of the cloud exciting the originally quiet regions and causing such vorticity-based structures to appear. Panel (i) shows the inside of the cloud for the SIC case where the homogeneous system actually decays slightly faster than the inhomogeneous case. This again points to the vortex energy being localized within the turbulent cloud and not dissipating to the out of cloud regions as shown by the homogeneous case. Both systems also have a greater decay as compared to panels (e) $N = 0.3$ and (g) $N = 0.6$ for within the cloud. The energy outside of the cloud for the SIC case as shown in panel (j) is also of the same magnitude as panels (d), (f) and (h) for the UIC cases.

3.1.4 Wave Energy
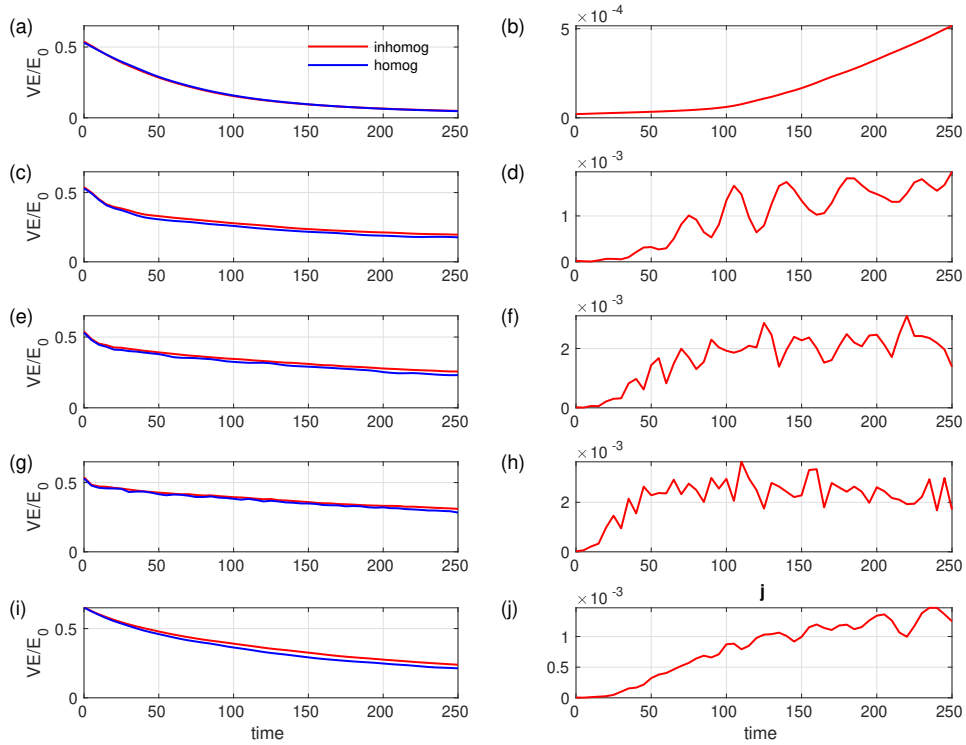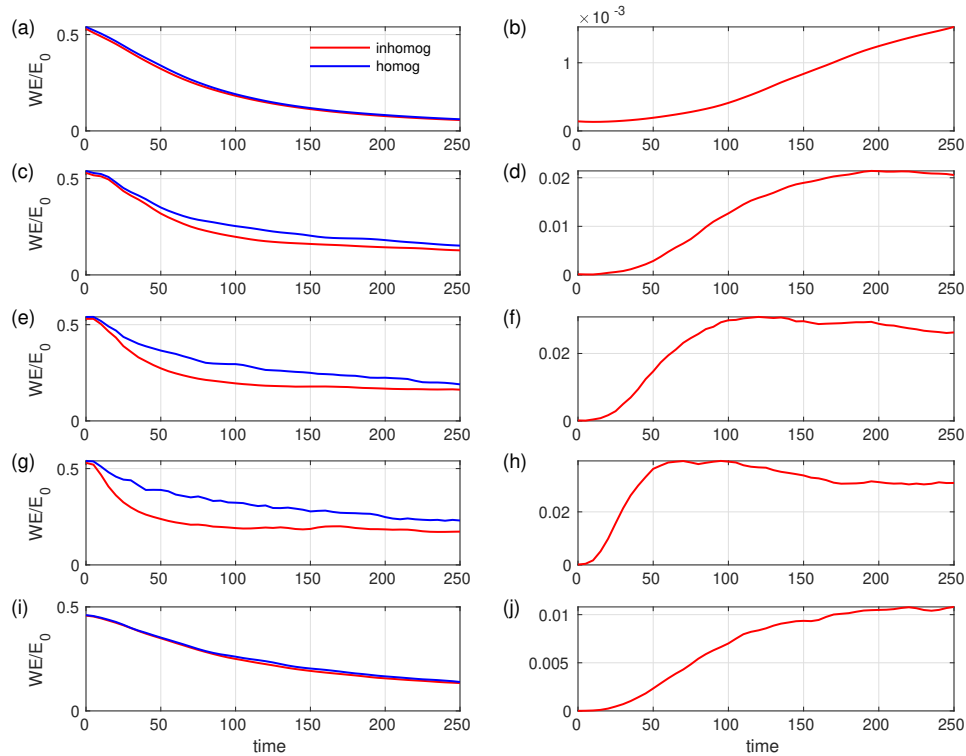

Figure 3.5: Time series of wave energy averaged over the defined cloud region for (a) $N = 0$, (c) $N = 0.15$, (e) $N = 0.3$, (g) $N = 0.6$, (i) $N = 0.3$(SIC) and outside the cloud region for (b) $N = 0$, (d) $N = 0.15$, (f) $N = 0.3$, (h) $N = 0.6$, (j) $N = 0.3$(SIC).

Figure 3.5 represents the wave energy inside the cloud (plots on the left) and outside the cloud (plots on the right), both normalized by the initial total energy inside the cloud for the homogeneous and inhomogeneous systems. It is observed that the inhomogeneous system has a greater decay of wave energy than the homogeneous system except in panel (i). This particular plot must be remembered as being initialized with initial conditions of $N = 0.3$ as compared to $N = 0$ for the other four on the left hand side of figure 3.5. This means that stratification wasn't applied at the start of the simulation and this continuous application of the same N results in a slower decay as compared to the other plots. It can also be stated that the wave energy in the cloud is lower than its homogeneous counterpart due to the inhomogeneity of that system. As the regions above and below the cloud are in no way as turbulent, waves will propagate much easier to these quiescent areas but this

will not be seen for the homogeneous setup as this difference in regions is not available. However, some revealing information is given by the results outside the cloud (plots on the right). A distinct increase in the wave energy can be seen to occur as well as a sustained amount of wave energy can be observed to be present outside of the cloud with the progress of time. The wave energy outside of the cloud also increases with larger N as panel (d) shows a peak at 0.02, panel (f) has values greater that 0.02 and panel (h) has the largest values of this set. In addition to this observation, there is more wave energy outside of the cloud, which is a whole magnitude of $O(10)$ larger, than there is vortex energy (figure 3.4) in the same region. This is quite telling to a significant presence of gravity waves being present in the once quiescent region. These results are also consistent to figures 3.3 and 3.4 as a movement of potential energy occurs from in the cloud to outside of the cloud whereas the vortex energy remains localized to within the cloud. Another observation is that the SIC case has a lot less wave energy out of the cloud than the UIC case with the same $N = 0.3$. This behaviour is also observed for the SIC case in figure 3.3. So, clearly the adjustment to stratification in the UIC case generates a lot of the waves that propagate out of the cloud.

3.2   Length Scales and Turbulence Parameters

3.2.1   Horizontal and Vertical Length Scales

Figure 3.6 shows the time series of the vertical and horizontal length scales for both inhomogeneous and homogeneous setups. It can be seen for early times $t \leq 100$, that the horizontal length scale l_h is smaller than the vertical length scale l_v (equation 2.11) in the UIC simulations, but similar in magnitude in the SIC simulation. At $t = 0$, $l_h \approx 1.2$ which is almost half of $l_v \approx 2.5$. Though the UIC simulations are initialized with $N = 0$ and expected to be isotropic in nature, these initial length scales do not abide by that. This can be due partially to an artifact of the window applied to compute the k_z spectra. However, the horizontal length scale increases with time as turbulence decays. This can be possibly due to the dominant eddies being bigger as the smaller eddies are decaying by the action of viscosity. However, such a trend is not as clearly observed for the vertical length scale. For the UIC simulations, l_v is found to fluctuate within a narrow range of values but decays somewhat steadily from 2.5 to close to 2 for the SIC simulation. It can also be noted that the initial l_v is almost equivalent to the final l_h for the SIC case. For the horizontal scales, the stratified simulations all show l_h growing in time as the turbulence decays but For l_v, such a trend is not as clear. In fact, there does not seem to be a significant dependence
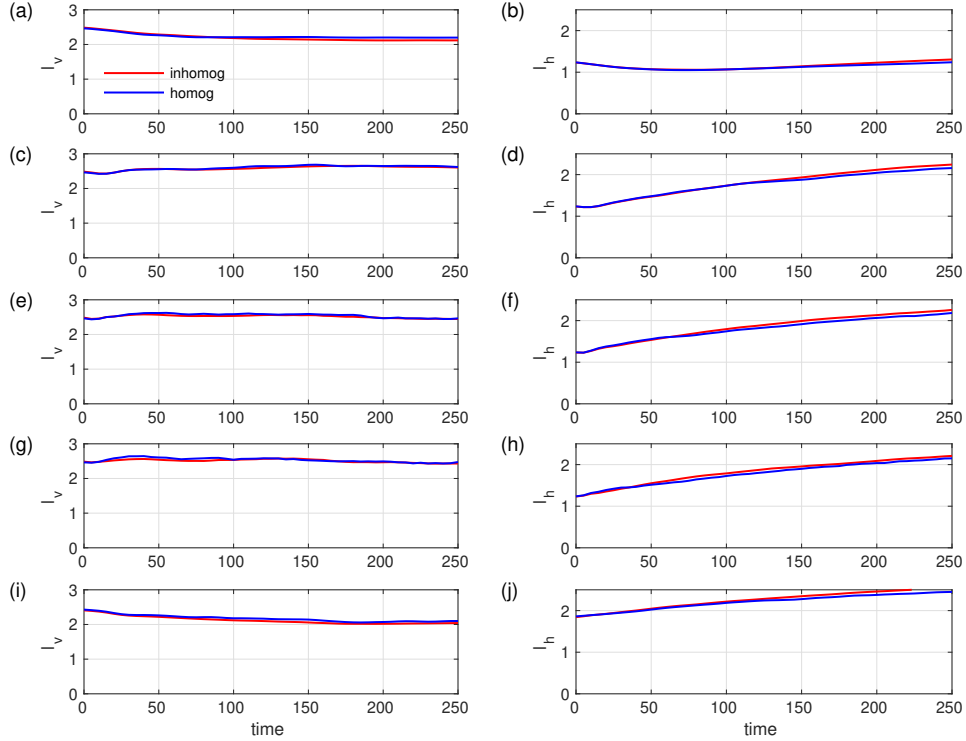
Figure 3.6: Vertical length scale for (a) $N = 0$, (c) $N = 0.15$, (e) $N = 0.3$, (g) $N = 0.6$, (i) $N = 0.3$(SIC) and horizontal length scale for (b) $N = 0$, (d) $N = 0.15$, (f) $N = 0.3$, (h) $N = 0.6$, (j) $N = 0.3$(SIC) in the cloud region.

of l_h or l_v on the stratification N. This offers a surprising result as it is expected, from previous work on homogeneous turbulence, that with time and varying N, these vertical lengths should adjust according to $l_v \sim U/N$ but this does not occur in these simulations.

3.2.2 Horizontal and Vertical Froude Numbers

Figure 3.7 displays a continuous decrease in both horizontal and vertical Froude numbers for increasing time with the inhomogeneous system decaying faster than the homogeneous one. It can also be immediately noticed that Fr_h and Fr_v are less than one. The small values of Fr_h are indicative of strongly stratified turbulence and suggests the possibility of achieving the $-5/3$ power-law relationship for the horizontal wavenumber energy spectra provided that $\mathcal{R}$ is large enough. Though much research has shown that $Fr_v \sim O(1)$ is found in strongly stratified turbulence, the results produced in this figure are more along

32
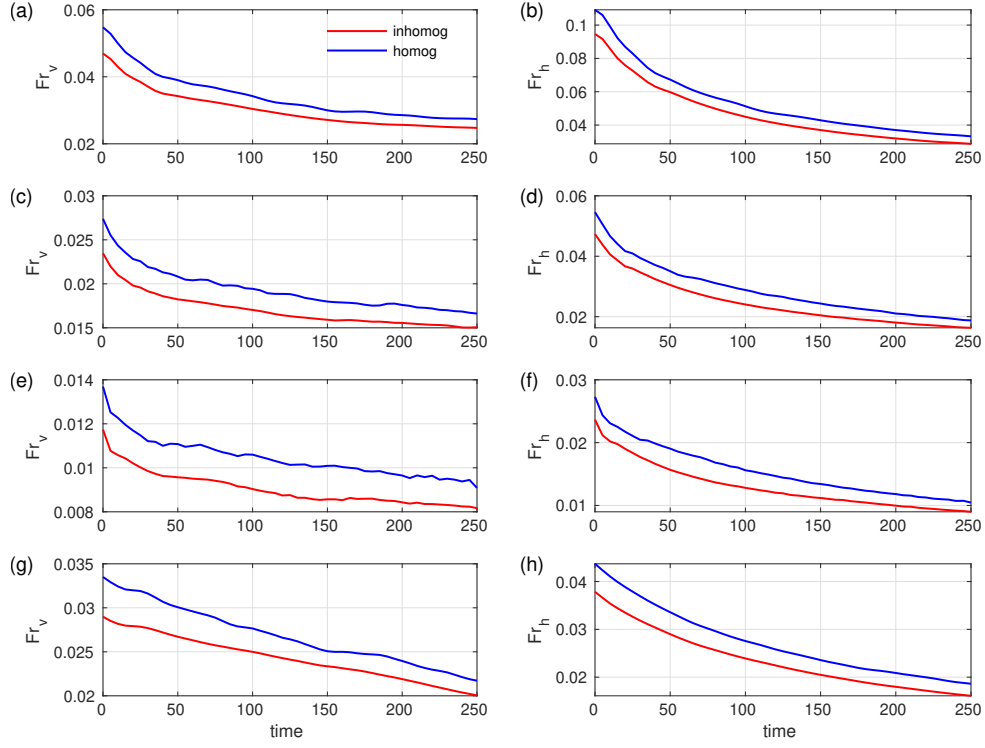
Figure 3.7: Vertical Froude number for (a) $N = 0.15$, (c) $N = 0.3$, (e) $N = 0.6$, (g) $N = 0.3$(SIC) and horizontal Froude number for (b) $N = 0.15$, (d) $N = 0.3$, (f) $N = 0.6$, (h) $N = 0.3$(SIC) in the cloud region.

the lines of $Fr_v \sim O(10^{-2})$. Furthermore, for both the UIC and SIC cases, the difference in the vertical Froude number at the beginning and end of the simulations is small which correlates to the somewhat constant value of l_v from figure 3.6. However, the Fr_v for the plots in panels (a), (c) and (e) can be seen to halve with a doubling of stratification which is expected for approximately constant l_v. One other point of observation is panel (g) which is the vertical Froude number for the SIC simulation. This particular plot is approximately linear for the Fr_v time series for both the inhomogeneous and homogeneous systems whereas the Fr_v time series for the UIC simulations exhibits nonlinear behaviour which can be seen at early times $t \leq 50$.
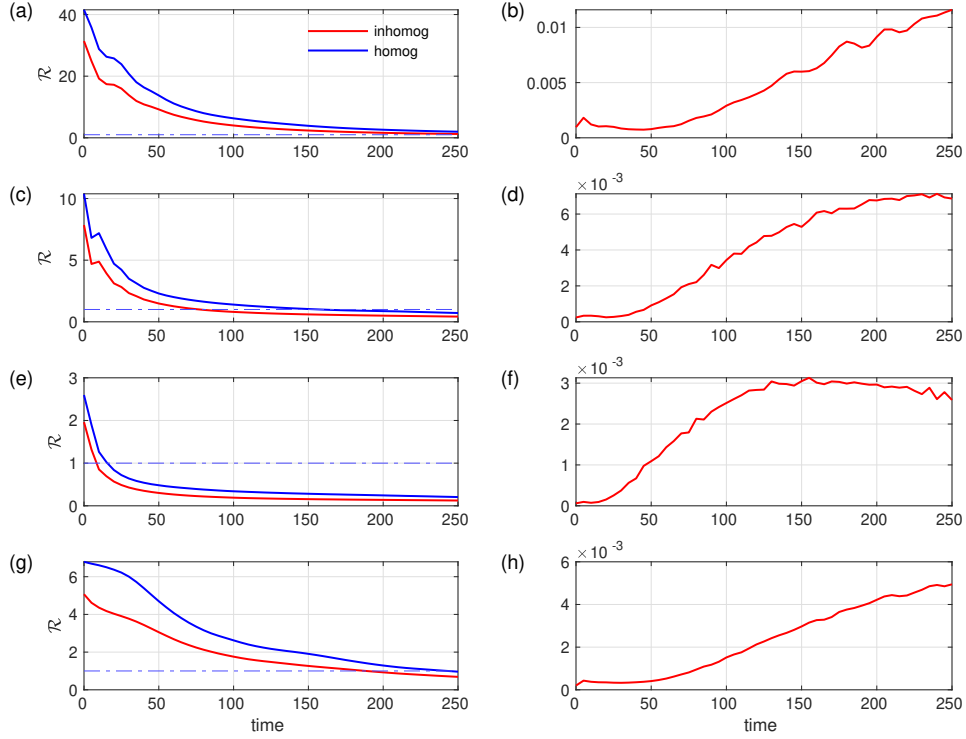
Figure 3.8: Buoyancy Reynolds number in the cloud for (a) $N = 0.15$, (c) $N = 0.3$, (e) $N = 0.6$, (g) $N = 0.3$(SIC) and out of the cloud for (b) $N = 0.15$, (d) $N = 0.3$, (f) $N = 0.6$, (h) $N = 0.3$(SIC). The dashed horizontal line in panels (a), (c), (e) and (g) is $\mathcal{R} = 1$.

3.2.3 Buoyancy Reynolds Number

In figure 3.8, the buoyancy Reynolds number $\mathcal{R}$ decreases faster in the cloud for the inhomogeneous simulations with UIC. It can also be noticed that the curves in panels (a), (c) and (e), which are the UIC simulations of increasing N, become increasingly steeper at earlier times in their descent to the reference value of $\mathcal{R} = 1$. This is expected as $\mathcal{R} \propto 1/N^2$. It can be seen that all simulations have $\mathcal{R} > 1$ at early times which coupled with the corresponding values of $Fr_h < 1$ indicate a strongly stratified turbulence system [Brethouwer et al., 2007]. A horizontal line at $\mathcal{R} = 1$ is plotted so as to trace at what time does the buoyancy Reynolds number dip below 1 into the viscous layered regime. For $N = 0.15$, $\mathcal{R} > 1$ for most of the simulation as seen in panel (a). For $N = 0.3$, it is above 1 for about 50 time units, which corresponds to 0.7 eddy time scales (table 2.1). For the largest $N = 0,6$, $\mathcal{R}$ drops below 1 rapidly and most out of the simulation is in the

viscous $\mathcal{R} < 1$ regime [Brethouwer et al., 2007]. For panels (a) and (c), the time for each of the homogeneous and inhomogeneous systems to go below 1 is approximately halved. An exception lies with panel (e) in that both systems go below 1 before $t = 25$ which is greater than half the time taken for the systems to exhibit such similar behaviour as in panel (c). These can be compared against the spectral plots below. Furthermore, a general increase in $\mathcal{R}$ occurs outside of the cloud albeit the values are quite small. Such an increase can happen due to the cloud now interacting with the once quiescent region. Moreover, a decrease of $\mathcal{R}$ can be seen for later times in panel (f). Given sufficient time, the right hand side plots will follow the decreasing pattern of their left hand side counterparts. The SIC case in panel (g) does not show such a steep decrease as its UIC counterparts and achieves a value of $\mathcal{R} = 1$ at t just greater than 100 and t just greater than 200 for the inhomogeneous and homogeneous systems respectively. In addition to this behaviour inside the cloud, the SIC case has energy of the same magnitude outside of the cloud, in panel (h), when compared to UIC cases in panels (d) and (f).

3.3 Dissipation

Within the cloud, figure 3.9 shows that the homogeneous system experiences a greater degree of dissipation than the inhomogeneous one within the cloud. If this is compared to figures 3.2-3.3 where the inhomogeneous system sees a quicker loss of kinetic and potential energies within the cloud, the behaviour in these figures are speculated to be associated to the propagation of waves rather than dissipation. It can also be seen that for greater N, the dissipation undergoes sharper decreases at earlier times which implies that viscosity comes to the forefront much faster for larger N. This is agreeable as strong stratification seeks to suppress the turbulence within the cloud facilitating the horizontal layering of intrinsic vortical structures. It should also be remembered that these vortical structures excite similar ones at a slightly smaller scale due to the vortex-stretching mechanism and this process continues as such. With this layering process being hastened by larger N, small enough vortical structures at the dissipation scale have been created at a quicker pace and viscosity acts on them at early times as $\mathcal{R} < 1$ (figure 3.8). Also, it can be noticed that the inhomogeneous system outside of the cloud experiences an increase in dissipation for panels (b) $N = 0$ and (d) $N = 0.15$. This is understandable as these regions are initially quiet and due to the evolution of the cloud, some activity is created outside of the cloud and dissipation soon ensued there. Moreover for panels (f) $N = 0.3$ and (g) $N = 0.6$ with stronger stratifications, a certain increase in dissipation is similarly seen but a decrease soon occurs at later times. Such a decrease is again greater for the case with the largest

35
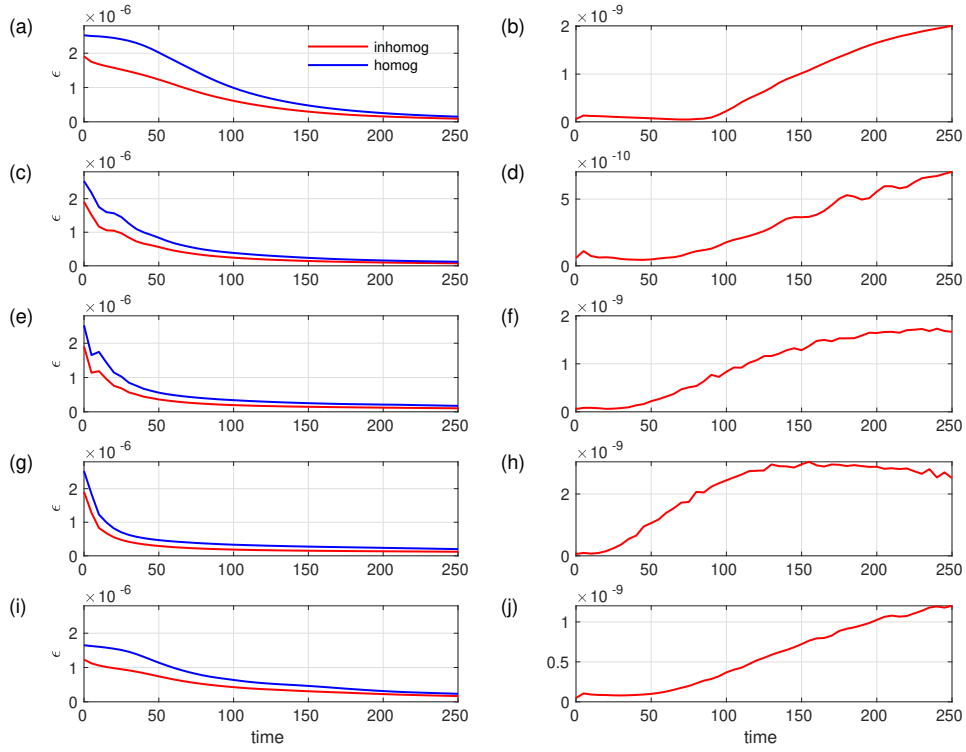
Figure 3.9: Dissipation in the cloud for (a) $N = 0$, (c) $N = 0.15$, (e) $N = 0.3$, (g) $N = 0.6$, (i) $N = 0.3(\mathrm{SIC})$ and out of the cloud for (b) $N = 0$, (d) $N = 0.15$, (f) $N = 0.3$, (h) $N = 0.6$, (j) $N = 0.3(\mathrm{SIC})$.

N. Given sufficient time, dissipation outside the cloud would also decrease and continue to do so as visualized in panel (g).

3.4   Cloud Evolution

In this section, changes in the vertical profiles of horizontally averaged energy is documented at particular times to extract important information in relation to the behaviour of the cloud. The plots are spaced 50 time units apart to map as much of the total evolution of the cloud for the length of time that the simulations were run.

Before an elaboration is provided for the evolution of energy inside and outside of the cloud, it may be helpful first to talk about how the shape of the cloud changes with time. For the $N = 0$ simulation (1st row), the cloud appears to get wider with increasing time
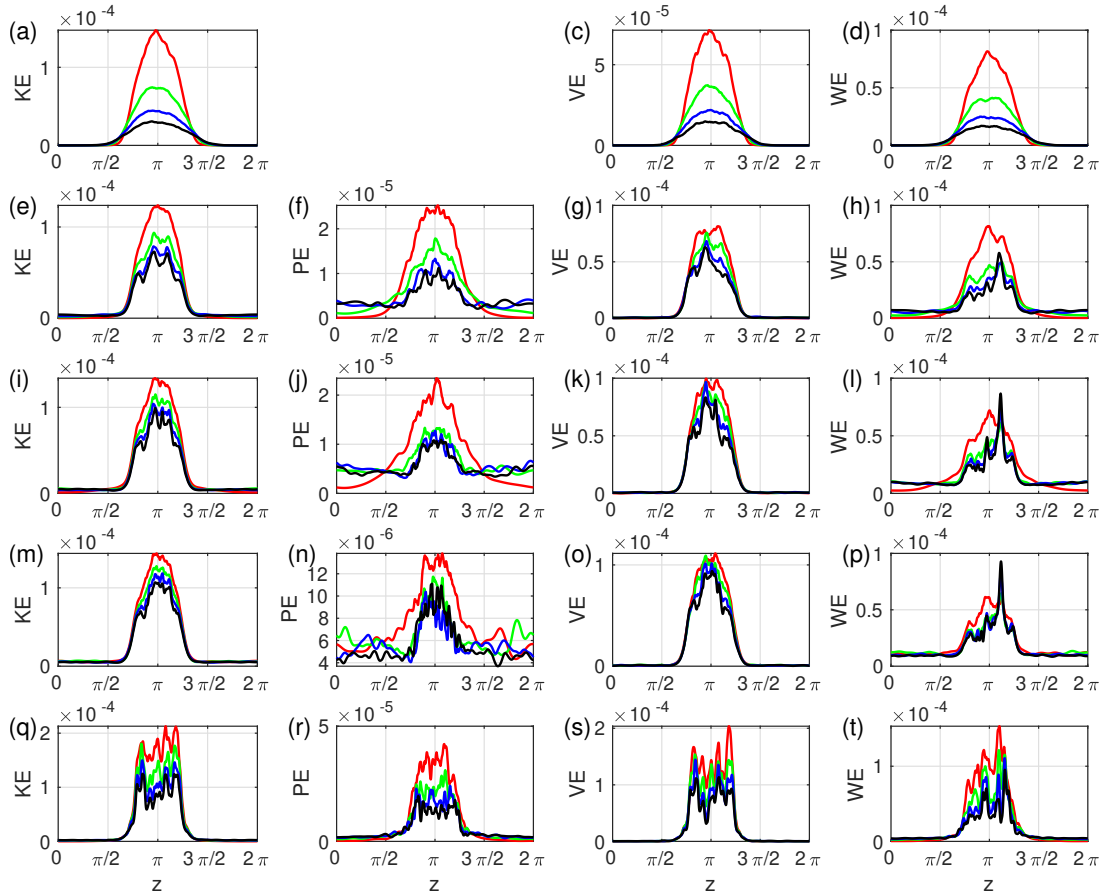
Figure 3.10: Horizontally averaged kinetic energy (1st column), potential energy (2nd column), vortex energy (3rd column) and wave energy (4th column) vs z at different times for $N = 0$ (1st row), $N = 0.15$ (2nd row), $N = 0.3$ (3rd row), $N = 0.6$ (4th row) and $N = 0.3$(SIC) (fifth row). The red curve is at $t = 50$, the green curve is at $t = 100$, the blue curve is at $t = 150$ and the black curve is at $t = 200$

but such an expansion is not observed for the stratified cases $N \neq 0$. This is expected as the presence of no stratification will not inhibit the spread of energy from the cloud to the upper and lower parts of the domain.

The first column of figure 3.10 shows the evolution of horizontally averaged kinetic energy with time for different N. There are a couple of features from panels (a), (e), (i), (m) and (q) which will help in understanding the effects of time and stratification on the kinetic energy. The first such feature is how the kinetic energy can affect the shape of

37

the cloud. The shape of the kinetic energy curves defined at the edges of the cloud region appear quite sharp and steep for panels (e), (i), (m) and (q). However, for $N = 0$ in (a), the kinetic energy curve is not as steep in its direction at the boundaries of the cloud. In fact, it can be seen that that width of the curve in (a) is slightly wider that the other four kinetic energy plots which infers that some amount of kinetic energy is present outside the defined cloud region. This is due to the absence of stratification which allows the cloud to expand freely due to the highly kinetic turbulent eddies. Where $N > 0$, stratification suppresses such vertical expansion as can be seek with kinetic energy being kept tightly within the cloud's boundaries. The second feature is how the amount of kinetic energy in the cloud changes with time. In (a), a clear decrease in the amount of kinetic energy within the cloud can be seen but this is again due to stratification not being present and allowing no inhibition of kinetic energy being spread over the quiescent areas due to the activity of the eddies, However, in the plots which boast of $N > 0$, there is no such clear decrease of kinetic energy within the cloud with the evolution of time. Additionally, as N becomes bigger, the decrease in kinetic energy with time becomes smaller. Stratification not only suppresses any vertical expansion of the turbulent cloud but also acts to keep the the majority of the kinetic energy within that same region [Riley and Metcalfe, 1987, Maffioli et al., 2014]). This also lends some further insight into how the rotational energy and divergent energy, the sum of which is the total kinetic energy within the cloud, are related to this situation. If the eddies and subsequent kinetic energy are being kept localized by the suppression of stratification, then it is a fair assumption that the vortex energy also has a similar localized behaviour within the cloud. Also, there should be an increase in wave energy outside of the cloud as the excitement of eddies play a part in the generation and propagation of waves. The vortex and wave energies will be further investigated in the third and fourth columns respectively. One noticeable difference between the UIC and SIC cases at $N = 0.3$ is the shape of the energy profile. The UIC case seems to be peaked in the centre of the cloud for all plotted times but the SIC case does not possess such a feature.

The second column of figure 3.10 shows the evolution of potential energy with time for different N. The panel (b) which represents $N = 0$ is absent as potential energy cannot be calculated for a system with zero stratification due to the lack of buoyancy. Moreover, the effects of non-zero stratification is important in observing the potential energy outside the cloud which is necessary in understanding any wave activity in the original quiescent areas. It can be seen that for all N, the amount of potential energy inside of the cloud decreases with time. This decrease is more significant that that observed for the kinetic energy. In addition to such a decrease, it can be seen that the potential energy curves widens to a range larger than the cloud's boundaries. Moreover, the decrease of this energy within the

38

cloud has a subsequent increase with time in the regions outside of the cloud. This points to the potential energy spreading throughout the domain with increasing time. Moreover, outside of the cloud, the amount of potential energy increases with larger N with the greatest out of cloud presence in panel (n). This contrasts with the kinetic energy plots where there was significantly less energy present outside of the cloud. Given $N > 0$ and the existence of potential energy outside of the cloud, these factors point to the presence of waves propagating through the non-cloud regions. The appearance of these waves can be confirmed in the physical space plots in one of the following sections. Regarding the SIC case, there is much less potential energy outside of the cloud when compared to UIC at $N = 0.3$. This is consistent with other results pointing to less wave energy excited by SIC case (figure 3.5).

The third column of figure 3.10 shows the evolution of vortex energy with time for different N. If panels (g) and (o) are compared, $N = 0.15$ vs $N = 0.6$, the difference between the curves become less distinct as there is more overlap. This infers that for larger N, the vortex energy within the cloud remains almost unchanging with the evolution of time. In other words, the vortex energy remains localized within the turbulent regions with little diffusion to outside of the cloud. This correlates to the kinetic energy plots (column 1 in figure 3.10) which was also localized to the cloud region. This implies that the decrease in the kinetic energy with time is due to the propagation of the divergent energy to the region outside of the cloud which means that the majority of energy in the once quiescent areas should be comprised of wave energy. Thus, this leads to an observation of the final column of plots which correspond to this wave energy.

The fourth column of figure 3.10 shows the evolution of wave energy with time for different N. It can be observed that the wave energy within the cloud decreases with time for all N. This decrease, however, get smaller for larger N. With the scrutiny of figure 3.10 thus far, it has been established that the kinetic energy is majorly composed of vortex energy which is localized to inside of the cloud which means they do not contribute much to happens on the outside. However, a significant increase in the potential energy outside of the cloud has been pointed out previously which lends to the supposition that there should also be a similar increase in the wave energy in the same regions. With this train of logic, the fourth column in the figure is investigated which does indeed present the existence of wave energy outside of the turbulent cloud. One difference when comparing the potential energy plots to the wave energy plots is the behaviour of the curves in the outside regions of the cloud. The potential energy plots are quite rough and jagged when compared to the smooth wave energy plots outside the cloud but it also worth noting that the scale of the former is much smaller than the latter. Also, there is a flat profile of wave energy outside the cloud at late time for panels (l) $N = 0.3$ and (p) $N = 0.6$ which does

not go to 0 like the vortex energy for the same regions. Also, as suggested in the potential energy panels (2nd column), there is less wave energy outside of the cloud for the SIC case than the corresponding UIC case for $N = 0.3$.

3.5   Physical Space Evolution

This section seeks to provide a visualization of the evolution of the turbulent cloud in physical space by extracting $x - z$ slices of the y-component of vorticity and the potential temperature perturbation. The y-component of the vorticity was chosen as it includes du/dz and therefore shows regions of strong shear. The vorticity component will reveal the evolution of eddy structures within the cloud as well as the degree of excitation created outside of the cloud. The potential temperature perturbation will aid in identifying any wave activity that is occurring outside of the cloud and well as providing a measure of how the potential and wave energies change within the cloud. For all plots with $N > 0$ in this section, three reference lines at 75°, 80° and 85° are drawn from the vertical and placed above and to the right of the cloud. These lines will assist in identifying the angles to which waves' crests and troughs are propagated in the regions outside of the cloud. However, the elaboration on these angles will be in section 3.7 which talks about the wave angle propagation.

Figure 3.11 shows the evolution of the y-component of vorticity for $N = 0$. This figure serves as a control when undergoing any comparison with the other cloud setups at various stratifications with $N > 0$. In these plots, $N = 0$ represents the evolution of an unstratified freely decaying turbulent cloud. Given sufficient time, the turbulent cloud would be uninhibited in its spread to the regions above and below it with the distinct possibility than it may completely dissipated before even reaching the bounds of the domain. The effect of stratification on this turbulent cloud will be seen in the subsequent plots within this section.

Figures 3.12 and 3.13 show the evolution of the y-component of vorticity and potential temperature perturbation respectively for $N = 0.15$. It is immediately communicable what leaps out in figure 3.12 and it is fair to extrapolate this observation convincingly to all the other plots with $N > 0$. The stratification acts as expected to limit the vertical spreading of the turbulent cloud and the general shape of it is maintained with increasing time. The phrase 'general shape' is used quite liberally here as the boundary of the cloud does expand a bit from panel (a) so that is not as clearly defined as it was at the beginning of the simulation. In figure 3.11 for $N = 0$, evidence of very large eddies, which are the size of the cloud, are seen moving up and down and spreading to the regions above and below where
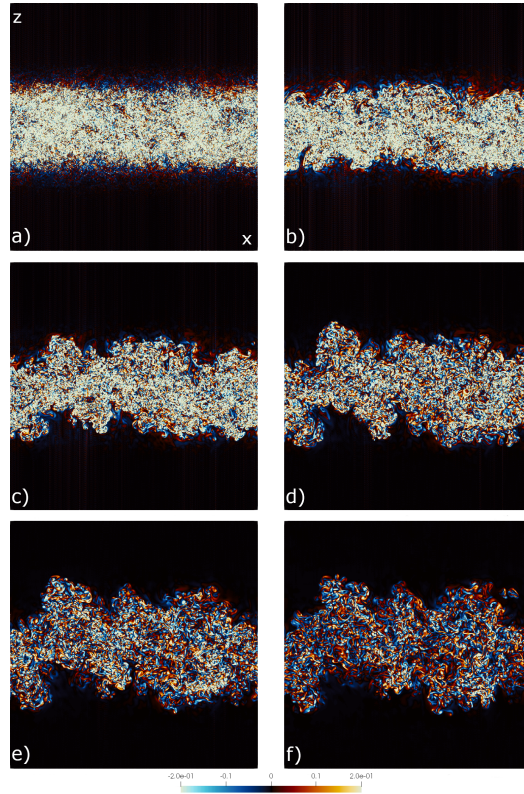
Figure 3.11: Vertical $(x - z)$ slices of the domain showing the y-component of vorticity for $N = 0$ at a) $t = 0$, b) $t = 50$, c) $t = 100$, d) $t = 150$, e) $t = 200$ and f) $t = 250$.

the cloud was originally initialized. This causes the broadening of the average thickness of the cloud. However, in figure 3.12 for $N = 0.15$, this spread does not occur. Instead, it can be seen that the large eddies collapse into pancakes with no 'meandering' of the large scales of the cloud as for $N = 0$ in figure 3.11. What is also visible is a lot of red and blue bands in the regions outside of the cloud which are propagating at a fairly consistent angle above and below the cloud. Not only do these bands indicate increased activity in the once quiet regions no doubt from excitation from the cloud, but their organisation suggests the action of propagating waves above and below the cloud. To complement the vorticity picture, figure 3.13 shows the potential temperature perturbations to emphasize the presence of any possible waves in the upper and lower parts of the domain. It can be seen the continuum of of colour outside of the cloud as seen in panels (a) and (b) in figure 3.13 starts to break up into patches as shown in panel (e). Such an organisation of these patches lends to the hypothesis that not only are internal waves being propagated
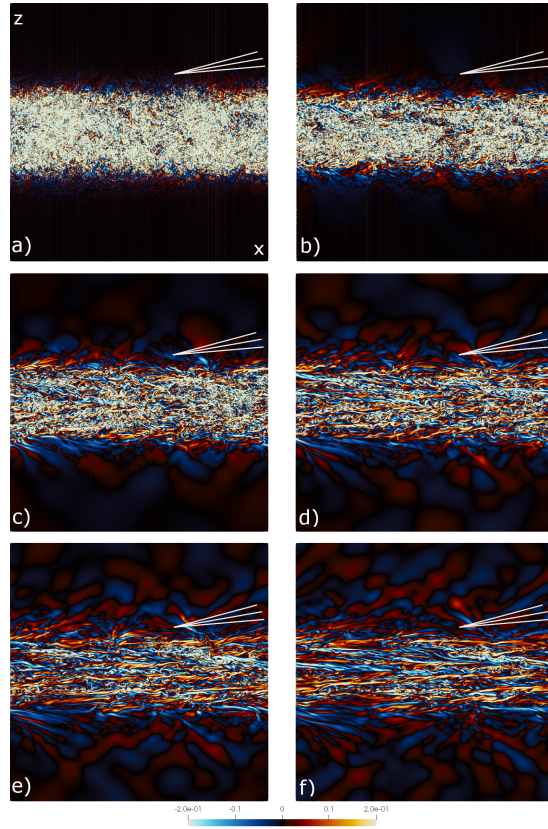
Figure 3.12: Vertical $(x - z)$ slices of the domain showing the y-component of vorticity for $N = 0.15$ at a) $t = 0$, b) $t = 50$, c) $t = 100$, d) $t = 150$, e) $t = 200$ and f) $t = 250$.

outside of the cloud but also that the angle of propagation of these waves can be calculated. Furthermore, it can be observed that within the cloud in figure 3.12, layers are beginning to form with time due to the vertical suppression of stratification.

Figures 3.14 and 3.15 show the evolution of the y-component of vorticity and potential temperature perturbation respectively for $N = 0.3$. The effect of increasing stratification is becoming more prominent with a larger N in figure 3.14 as compared to figure 3.12. The layers within the cloud are forming in shorter amounts of time and are quite distinct in panel (e) where $t = 200$ with reference to panel (f) where $t = 250$ in figure 3.12. Furthermore, the activity outside of cloud is at a greater level as a somewhat uniform distribution of the red and blue bands is becoming more and more apparent. The degree of the spread of these bands can be better appreciated in figure 3.15 where it not only forms in shorter times but
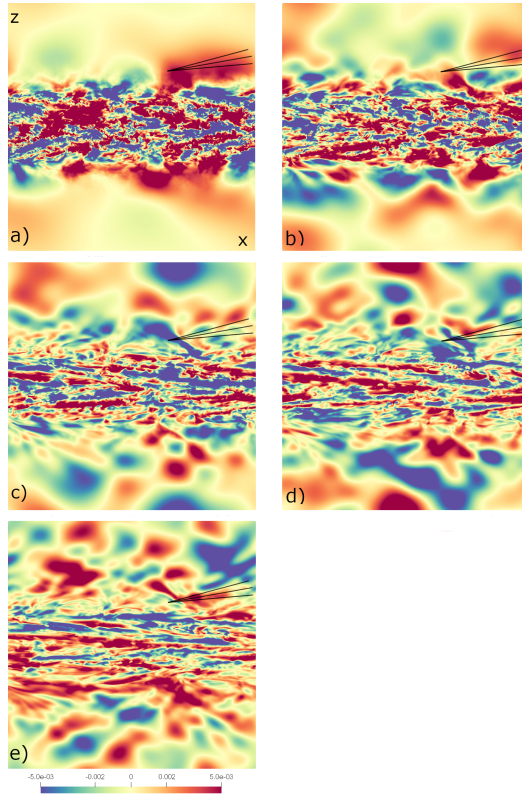
Figure 3.13: Vertical $(x - z)$ slices of the domain showing the potential temperature perturbation in the domain for $N = 0.15$ at a) $t = 50$, b) $t = 100$, c) $t = 150$, d) $t = 200$ and e) $t = 250$.

the quantity of them is greater. In particular for panels (e) and (f), there are some bands just around the border of the cloud that are in a position that coincides particularly with the 85° reference line. This is extremely encouraging and a further investigation of this observation will be pursued in the next section. This arrangement of patchiness indicates to a stronger presence of propagating waves above and below the cloud. These observations of the more pronounced layering within the cloud as well as the greater out of cloud wave activity in figures 3.14 and 3.15 when compared to figures 3.12 and 3.13 are due to the increased N. With this train of thought, the plots for $N = 0.6$ ought to have even stronger features.

Figures 3.16 and 3.17 show the evolution of the y-component of vorticity and potential temperature perturbation respectively for $N = 0.6$. Increasing the stratification even
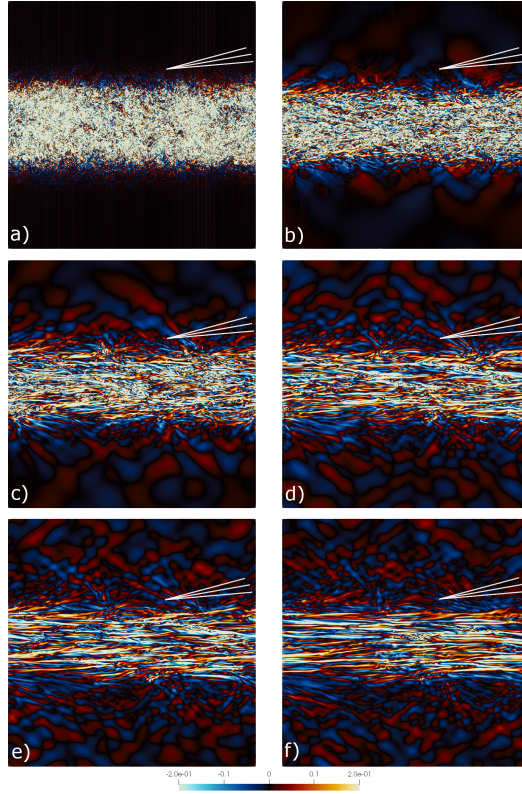
Figure 3.14: Vertical $(x - z)$ slices of the domain showing the y-component of vorticity for $N = 0.3$ at a) $t = 0$, b) $t = 50$, c) $t = 100$, d) $t = 150$, e) $t = 200$ and f) $t = 250$.

further, as in figure 3.16, gives rise to two important features. The first is that the layers are well formed, smooth and distinct in their structures within the cloud. The second is the propagating of waves into the regions above and below the cloud. For early times as in panel (b), some wave activity can be seen almost filling the entire domain. Such a spread was not observed at a similar time for figures 3.12 and 3.14 which directly relates to the impact of very strong stratification. To further investigate any such wave activity, figure 3.17 is utilized. It is in these figures that the effects of very strong stratification are felt. In panel (e) of figure 3.15, the region of the cloud can still be distinguished but not as much for panel (e) in figure 3.17. It can be seen that the shape of the cloud has almost completely disintegrated with the evolution of time. What this indicates is that the amplitude of the potential temperature perturbations outside the cloud are just as big as inside the cloud. This points to a strong presence of wave energy existing in the out of cloud regions. There is a thorough spread of the potential temperature perturbation throughout the domain

44

Figure 3.15: Vertical $(x - z)$ slices of the domain showing the potential temperature perturbation in the domain for $N = 0.3$ at a) $t = 50$, b) $t = 100$, c) $t = 150$, d) $t = 200$ and e) $t = 250$.

with nothing centralized within the bounds that define the cloud. The uniformity of the red and blue patches outside of the cloud as seen in figures 3.12-3.14 is facilitated much quicker in the case $N = 0.6$ again, unsurprisingly, to the larger N and hence, greater wave activity. Observing the edges of the cloud in both figures display structures that are in agreement with the the angular reference lines as with the $N = 0.3$ case.

Figures 3.18 and 3.19 show the evolution of the y-component of vorticity and potential temperature perturbation respectively for $N = 0.3$(SIC) and will be compared to figures 3.14 and 3.15 which have the same stratification but with UIC. Comparing panels (b) and (c) in figures 3.14 and 3.18, $N = 0.3$(UIC) seems to possess bands outside of the cloud at earlier times than $N = 0.3$(SIC). This is what should be expected since the adjustment of the initially unstratified turbulence to evolve under stratification in the UIC simulation
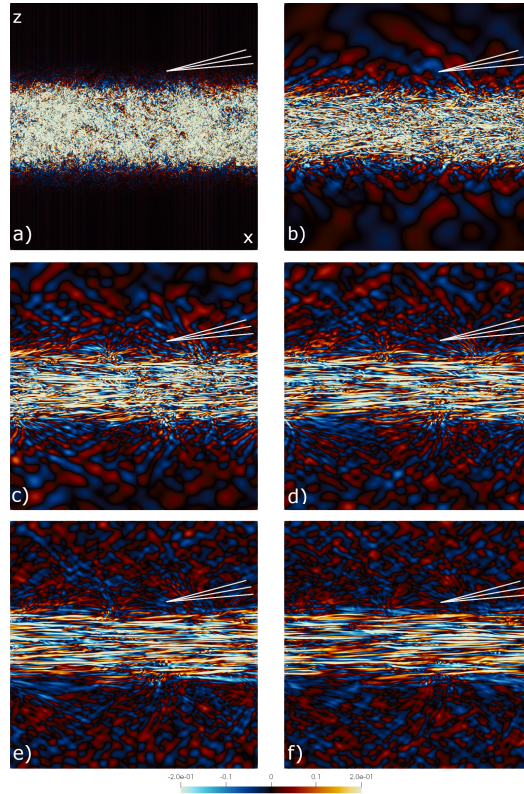
Figure 3.16: Vertical $(x - z)$ slices of the domain showing the y-component of vorticity for $N = 0.6$ at a) $t = 0$, b) $t = 50$, c) $t = 100$, d) $t = 150$, e) $t = 200$ and f) $t = 250$.

will have more vertical velocity, and therefore excite more waves than the already initially stratified turbulence in the SIC simulation. Furthermore, for the same panels (b) and (c) in both figures, a greater degree of layering of the eddies at earlier times can be seen for the SIC case than the UIC run and a final observation of panel (e) shows the final layers are much more developed and distinct for the SIC simulation. This can also be attributed to the fact that the SIC simulation was initialized with stratified turbulence. To confirm this greater wave activity outside of the cloud at earlier times for the UIC simulation, the potential temperature perturbation in figures 3.15 and 3.19 is investigated. Referring now to panels (b) and (c) in these figures show immediately a greater colour intensity and spread of the patches outside of the cloud for the UIC case when compared to the SIC simulation. This does indeed cement the fact that the UIC simulation has greater wave activity outside the cloud at earlier times. The prominence of wave activity outside of the cloud for the UIC run continues for increasing time as shown in panel (e) but it is
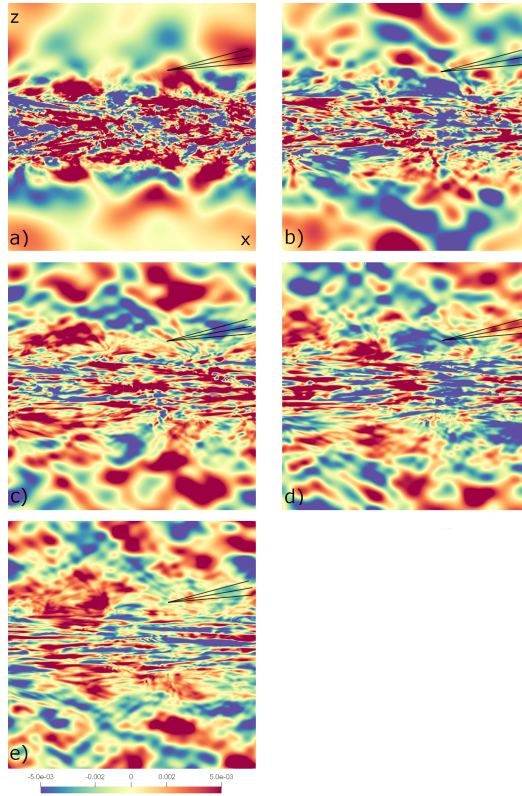
46

Figure 3.17: Vertical $(x - z)$ slices of the domain showing the potential temperature perturbation in the domain for $N = 0.6$ at a) $t = 50$, b) $t = 100$, c) $t = 150$, d) $t = 200$ and e) $t = 250$.

worth noting that the patches outside the cloud for the SIC simulation is thinner and more elongated for all times than its UIC counterpart. This possession of greater wave activity for the UIC simulation can also seen in figure 3.3 where the potential energy outside the cloud for the SIC case was an entire magnitude smaller than that of the UIC simulation. One final point to appreciate is the orientation of structures in both figures at the edges of the cloud which is in agreeement with the angular reference lines.

It has been observed in this section that for increasing N, there is greater activity occurring outside of the cloud at earlier times. In particular, the wave presence outside of the cloud becomes significantly stronger as N in increased from 0.15 to 0.6 so much so that there is almost no distinguishing factor for the degree of the potential temperature perturbation for the $N = 0.6$ case. A comparison between the UIC simulation and the SIC
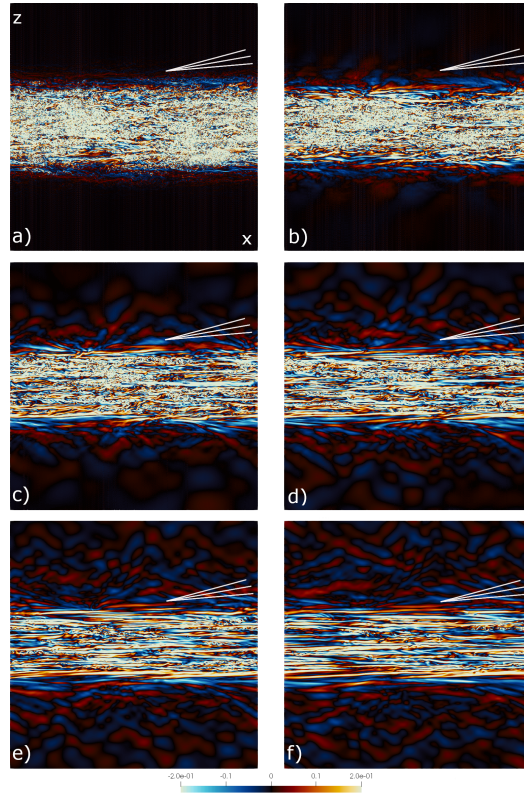
Figure 3.18: Vertical $(x - z)$ slices of the domain showing the y-component of vorticity for $N = 0.3$(SIC) at a) $t = 0$, b) $t = 50$, c) $t = 100$, d) $t = 150$, e) $t = 200$ and f) $t = 250$.

simulation for $N = 0.3$ highlighted that the former had a greater amount of waves being present at earlier times outside of the cloud than the latter. Moreover, as the stratification changed from $N = 0.3$(UIC) to $N = 0.6$ and then $N = 0.3$(SIC), it appears as though that different types of waves may be present in the domain. There seems to be one type of wave near the edges of the cloud and another type far away towards the upper and lower bounds of the domain. This possible difference will be explored further in section 3.7 which elaborates on the wave angle propagation.
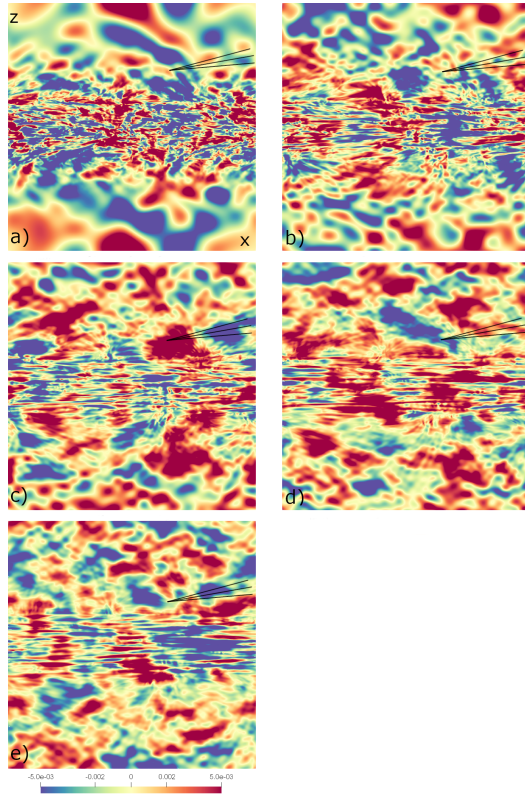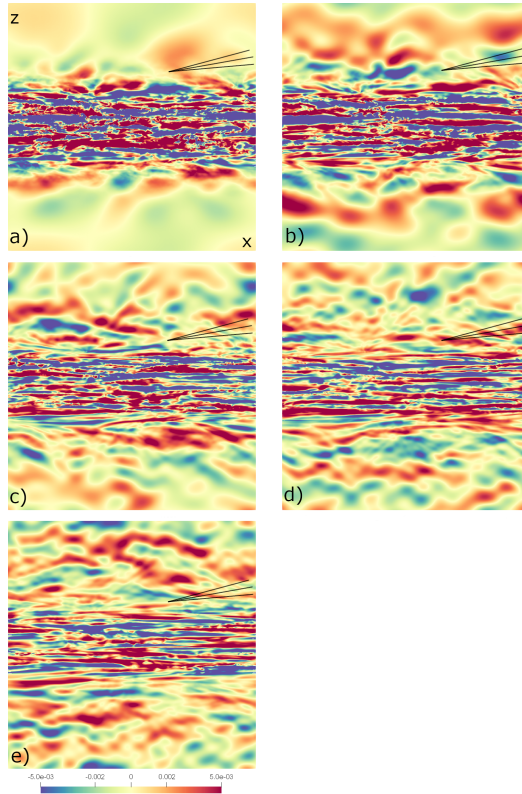
Figure 3.19: Vertical $(x - z)$ slices of the domain showing the potential temperature perturbation in the domain for $N = 0.3$(SIC) at a) $t = 50$, b) $t = 100$, c) $t = 150$, d) $t = 200$ and e) $t = 250$.

3.6 Spectra

3.6.1 Horizontal Spectra

This subsection is dedicated to analysing the horizontal wavenumber spectra of the total energy, which is the sum of the kinetic and potential energies, in and out of the cloud for both inhomogeneous and homogeneous systems. The total energy is used for this spectral analysis as it provides a simple yet thorough primary approach in investigating how the inhomogeneous system compares to results derived from homogeneous turbulence. Furthermore, using the total energy spectra allows for a reasonable number of plots to be included in this study which facilitates a more focused discussion of the results. All plots in this subsection contain a line of slope $-5/3$ at the top right so as to be able to

49

compare to the slope of the spectra at varying ranges of horizontal wavenumbers. 'OC' in labelled in the plots within this section to refer to the energy outside of the cloud in the inhomogeneous simulations. Wherever appropriate, the buoyancy wavenumber k_b, the Ozmidov wavenumber k_O and the Kolgomorov or dissipation wavenumber k_d are labelled as dashed vertical lines on the figures in both the horizontal and vertical spectra sections.

Figure 3.20: Horizontal wavenumber spectra of total energy in and out of the cloud for $N = 0$ at (a) $t = 50$, (b) $t = 100$, (c) $t = 150$ and (d) $t = 200$. 'OC' is the energy outside the cloud for the inhomogeneous system.

Figure 3.20 shows the total horizontal wavenumber energy spectra for the simulations with $N = 0$. A similar evolution of energy within the cloud for both the homogeneous and inhomogeneous systems is observed but with the latter having slightly lower energy for all plotted times. This is likely due to the window that is applied to the initial conditions to make the cloud, which reduces the energy near the top and bottom of the cloud compared to the homogeneous case. At all times, there is steepening beyond $-5/3$ at large wavenumbers which is expected near the dissipation wavenumber k_d. It can also be seen that the inhomogeneous energy outside of the cloud increases with time and also assumes a similar

shape to the curves representing the energy within the cloud but with smaller amplitude. This is a fairly straightforward expectation as there is no stratification present for these plots and the cloud is thus uninhibited in its vertical spread to the regions above and below the cloud. It may even be the case that with sufficient time, all the turbulence will decay away without even reaching the bounds of the domain. One final observation for figure 3.20 is that there exists a range of wavenumbers for which all spectra has an approximate $-5/3$ gradient; careful inspection will reveal a slope that is slightly shallower than $-5/3$. The energy in the cloud has such a range for all plotted times but only for later times as shown in panels (c) and (d) that the inhomogeneous energy outside the cloud exhibits such a range of wavenumbers. This is again due to the spreading of the once defined turbulent cloud into the regions above and below it.
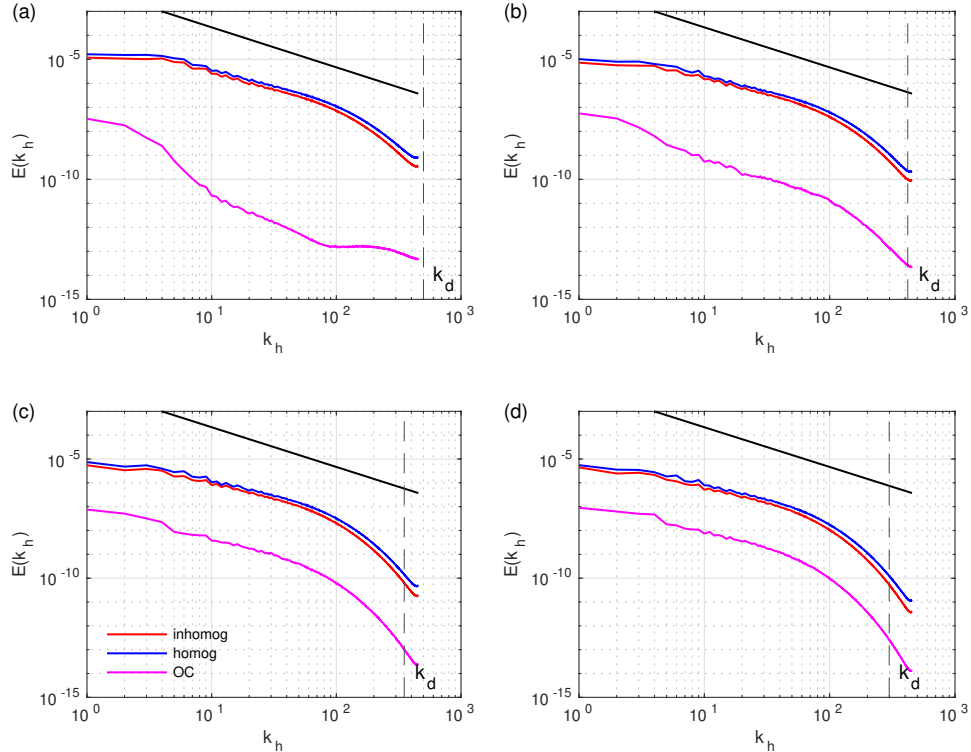

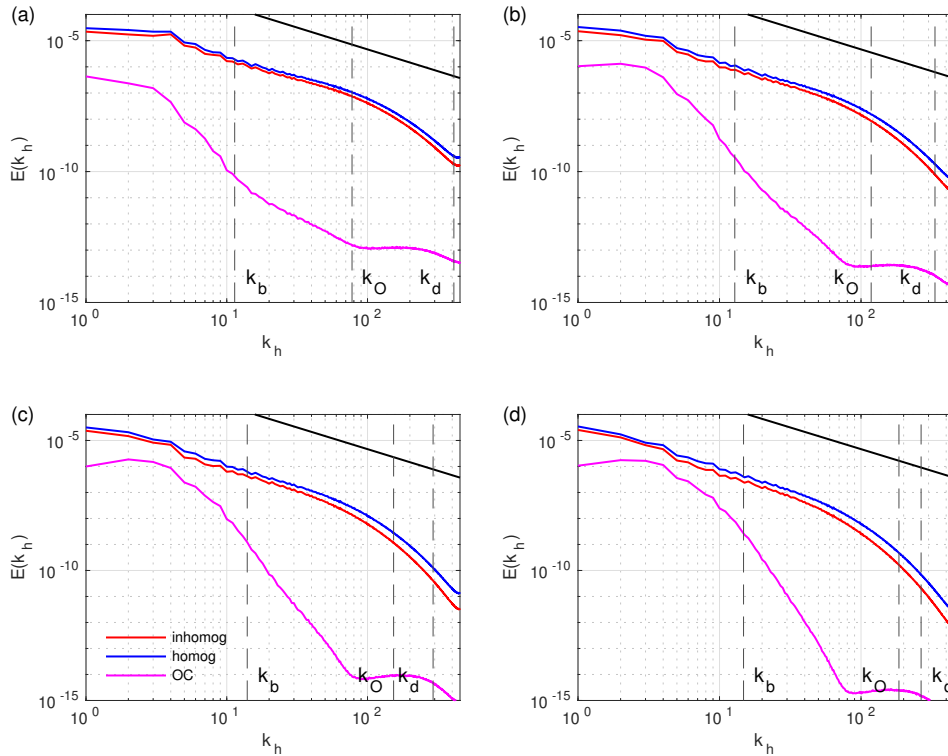Figure 3.21: Horizontal wavenumber spectra of total energy in and out of the cloud for $N = 0.15$ at (a) $t = 50$, (b) $t = 100$, (c) $t = 150$ and (d) $t = 200$. 'OC' is the energy outside the cloud for the inhomogeneous system.

Figure 3.21 shows the total horizontal wavenumber energy spectra for the simulations with $N = 0.15$. Both the homogeneous and inhomogeneous systems have similar spectral

51

shapes throughout the wavenumber range for all times plotted. One difference, however, is the the inhomogeneous system has a lower energy content than the homogeneous one due to the window function. For panels (a) and (b) which corresponds to earlier times of the simulation, it can be seen that the spectral slope is indeed similar to $-5/3$ by comparing it to the straight black line at the top right of the plots. This $-5/3$ spectral slope is maintained down to the Ozmidov wavenumbers but starts to fall away in a steeper manner in the dissipation range, which moves to smaller wavenumbers as time progresses. Panels (c) and (d) display and initial agreement to the $-5/3$ reference line for the first part of the buoyancy-Ozmidov range of wavenumbers but then progresses in a steeper manner around $k_h \sim 100$. This can be attributed to k_d getting smaller as ϵ decreases, so viscous effects are felt at smaller k_h. Another point to note is the energy outside of the cloud for the inhomogeneous system. The slope of this curve have no relation to $-5/3$ as it is much too steep which is expected due to the small value of $\mathcal{R}$ outside of the cloud (figure 3.8). It is also worth noting that the large-scale energy outside of the cloud, identified as the maximum in the spectra, is seemingly similar to that inside of the cloud at $k_h = 3 - 4$ at late times. This is shown in panel (d). However, this is a log-log plot which means that this max value of the 'OC' curve is still quite smaller than the energy of the in-cloud spectra at the same wavenumber. In spite of this, it gives insight that stronger stratification may bring this max value closer to that in the cloud at a particular wavenumber.

Figure 3.22 shows the total horizontal wavenumber energy spectra for the simulations with $N = 0.3$. Both the inhomogeneous and homogeneous systems exhibit similar spectral behaviour in the cloud with one immediate difference being that the inhomogeneous system deviates from the homogeneous system at larger wavenumbers. This deviation gets bigger and steepens for increasing time. This difference is much more pronounced in figure 3.22 than the more weakly stratified case in figure 3.21. Another observation is that the inhomogeneous system possesses less energy than the homogeneous one for all plotted wavenumbers, as in the above cases. Two salient points are to be mentioned here. Firstly, the long power-law from small k_h to medium k_h is actually a little steeper than $-5/3$, unlike above (figure 3.21) where it was slightly shallower. Secondly, it has been noticed in the above figure 3.21 and in this one that the steepening of the spectra in the dissipation range moves to smaller k_h with increasing time. This is due to the changing value of the buoyancy Reynolds number $\mathcal{R}$ (figure 3.8) and its relationship to k_O and k_d namely $\mathcal{R} = (k_d/k_O)^{4/3}$ or equivalently $\mathcal{R}^{3/4} = (k_d/k_O)$. Thus, when $\mathcal{R} < 1$ and is raised to a fractional power, the result is that $k_O > k_d$ which means that the dissipation range now advances to smaller wavenumbers. Thus, in terms of the reference line of slope $-5/3$, the spectral curves fall away more steeply than $-5/3$ at at smaller wavenumbers as viscous effects are now felt at these scales. The final observation to be made here is the energy outside of the cloud. This
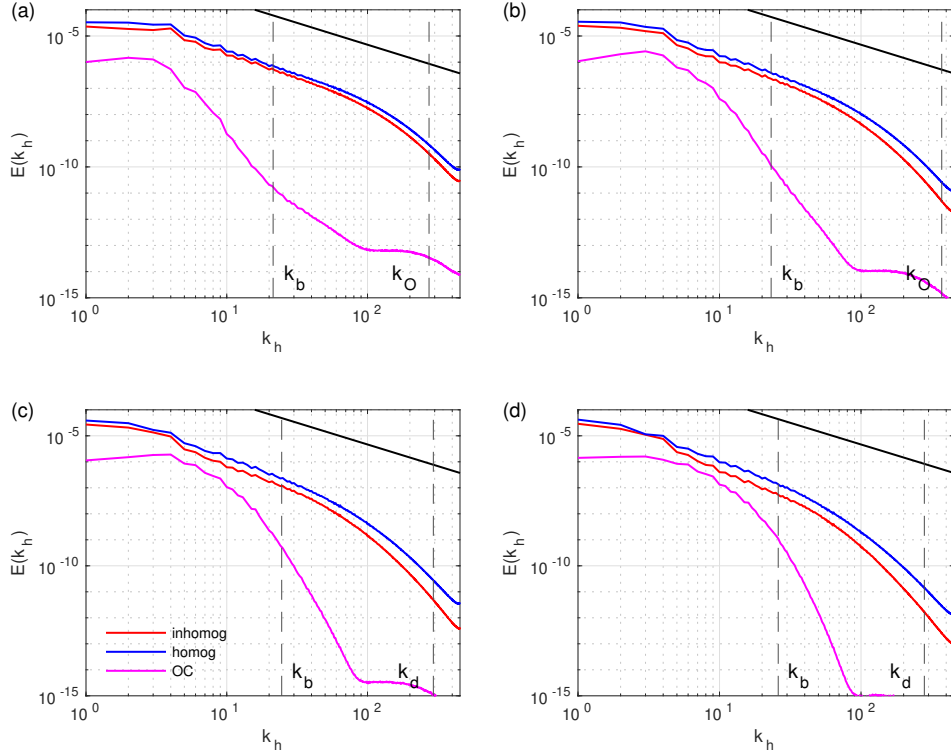
Figure 3.22: Horizontal wavenumber spectra of total energy in and out of the cloud for $N = 0.3$ at (a) $t = 50$, (b) $t = 100$, (c) $t = 150$ and (d) $t = 200$. 'OC' is the energy outside the cloud for the inhomogeneous system.

'OC' curve is much steeper than the $-5/3$ reference line and this can be reiterated as being a result of $\mathcal{R}$ being small outside of the cloud (figure 3.8). Panel (d) shows quite a close similarity between the max of the out of cloud spectra and in-cloud spectra at wavenumber $k_h = 3 - 4$. The values of these maxima are actually closer that those shown in panel (d) of figure 3.21 and indicates an increase in energy out of the cloud when the stratification is doubled. It should be remembered that is only a qualitative observation as this log-log plot doesn't truly indicate quantitatively these energies at $k_h = 3 - 4$.

Figure 3.23 shows the total horizontal wavenumber energy spectra for the simulations with $N = 0.6$. It continues the tale from figures 3.21-3.22 where the inhomogeneous system does indeed possess less energy that the homogeneous system in the cloud, as in the previous cases, but immense scrutiny is now placed on the slope of the spectra in this figure 3.23. The slope only possesses a $-5/3$ slope for wavenumbers smaller that k_b at early times in panel (a). As time increases further in panels (b)-(d), the spectra becomes steeper
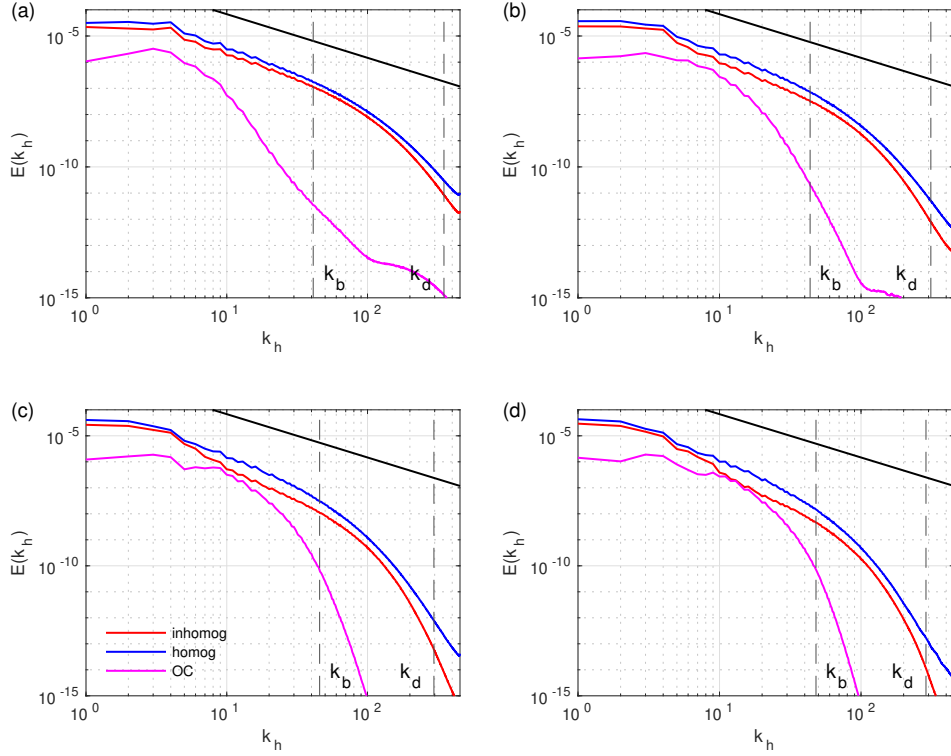
Figure 3.23: Horizontal wavenumber spectra of total energy in and out of the cloud for $N = 0.6$ at (a) $t = 50$, (b) $t = 100$, (c) $t = 150$ and (d) $t = 200$. 'OC' is the energy outside the cloud for the inhomogeneous system.

than $-5/3$ for $k_h < k_b$. Referring back to figure 3.8, this does not come as a surprise as $\mathcal{R}$ almost immediately drops below 1 for the $N = 0.6$ simulation at early times. Thus it can be expected that the entire spectra will be steeper than $-5/3$ from the same early times. Another point to notice is that k_O is not labelled in the plots. This is again due to the relation $k_d/k_O = \mathcal{R}^{3/4}$ so when $\mathcal{R} < 1$, the ratio of k_d to k_O changes and hence their order in the wavenumber range also swaps. One outstanding revelation and certainly a most welcome one is the now quite close relationship between the out of cloud and inside the cloud maximum large-scale energies. The distance between is much closer than before (figures 3.21-3.22) with the curves actually overlapping for a narrow band of wavenumbers around $k_h \sim 10$ for panel (d) in figure 3.23. This is quite a significant observation as it tells that the simulation with the largest N and sufficient time, the energy outside of cloud is equivalent to that in it. This alludes to the possible strong presence of internal waves being propagated into the regions outside of the cloud as well as, to an extent, the turbulence in

the cloud exciting the regions beyond its boundaries.
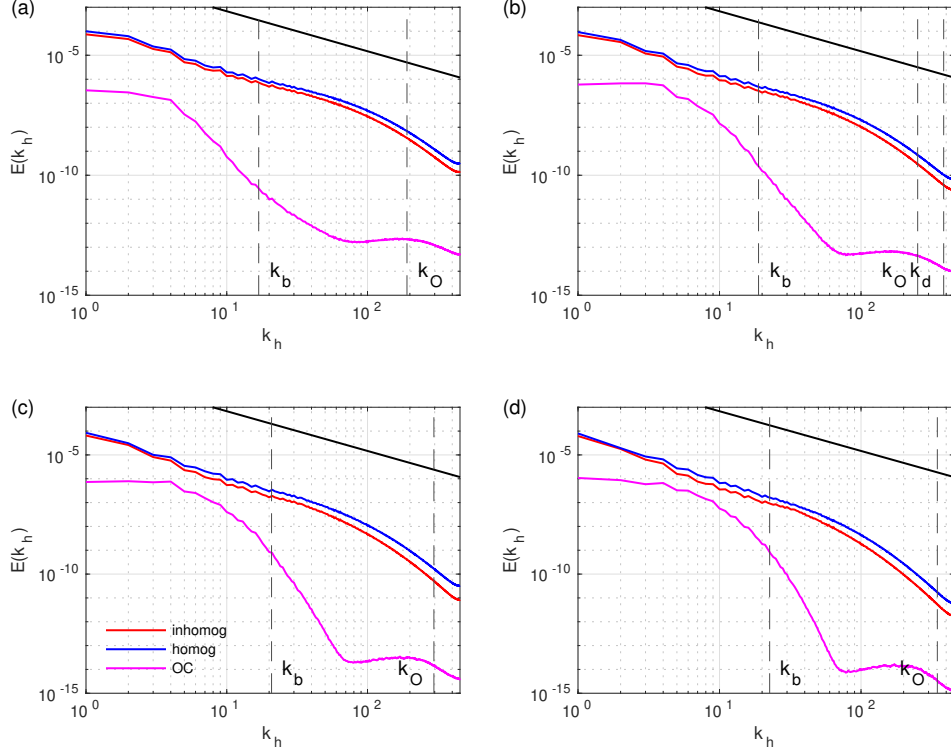
Figure 3.24: Horizontal wavenumber spectra of total energy in and out of the cloud for $N = 0.3(\text{SIC})$ at (a) $t = 50$, (b) $t = 100$, (c) $t = 150$ and (d) $t = 200$. 'OC' is the energy outside the cloud for the inhomogeneous system.

Figure 3.24 shows the total horizontal wavenumber energy spectra for the simulations with $N = 0.3(\text{SIC})$. Again, as in figures 3.20-3.23, that energy within the cloud is almost equivalent for both the homogeneous and inhomogeneous simulations with the latter having less energy, as in the previous cases, and deviating slightly from the former especially at the largest wavenumbers around the Ozmidov wavenumber. It is also noteworthy that in panels (a)-(c), there is a great agreement with the slope of the spectra with respect to the $-5/3$ reference line. It is also important that the impact of the initial conditions be studied by comparing $N = 0.3(\text{UIC})$ in figure 3.22 and $N = 0.3(\text{SIC})$ in figure 3.24. It can be seen that for earlier times by comparing panels (a)-(c) in both figures that the SIC simulation has a much better agreement to the $-5/3$ slope than the UIC simulation. This is due to $\mathcal{R} \leq 1$ at later times for $N = 0.3(\text{SIC})$ than for $N = 0.3(\text{UIC})$ as shown in figure 3.8. It is for this same reason that at later times in panel (d) for both figures, k_d appears

at a smaller wavenumber along with the effect of viscosity for the UIC case than the SIC case for $N = 0.3$. Out of all the horizontal wavenumber spectra plots, figures 3.21 and 3.24 boast of a substantial agreement to the $-5/3$ reference line. Again, this is due to the fact that $\mathcal{R}$ takes the longest time to decrease to 1 (figure 3.8) for both these cases as compared to the $N = 0.3$ run in figure 3.22 and the $N = 0.6$ run in figure 3.23. Furthermore, there is a peak in the energy spectra for the inhomogeneous system outside of the cloud at $k_h = 3 - 4$ where the max energy is quite similar but still less than to what is in the cloud. As always, it is an ever appreciated reminder that this is a log-log plot but what it does offer is a comparison to the $N = 0.3$(UIC) case. Inspecting figures 3.22 and 3.24, the peak of the out of cloud energy is closer to the in-cloud energy for $N = 0.3$(UIC) than for $N = 0.3$(SIC). Additionally, the inhomogeneous system in the cloud for the SIC simulation does not see such a decrease of energy when contrasted against the UIC simulation. Also, at larger wavenumbers, this out of cloud spectrum plummets to a gradient much steeper than $-5/3$ due to $\mathcal{R}$ outside of the cloud is much less 1.

The overall trend that can be observed for these horizontal spectra plots (figures 3.20-3.24) is the relationship they hold with the buoyancy Reynolds number (figure 3.8). For a sufficiently large $\mathcal{R}$, the spectral plots follow along with a slope of $-5/3$. However, greater stratifications showed that $\mathcal{R}$ dipped below 1 much more quickly and this is reflected in the spectral plots of increasing N in that the spectra becomes steeper at earlier times when compared to the $-5/3$ line. This point becomes quite conspicuous for figure 3.23 in that all plots start to become steeper than $-5/3$ for increasingly smaller wavenumbers due to the advancement of the Kolmogorov wavenumber with the evolution of time. This also coincides with the fact that the simulation with $N = 0.6$ dives below $\mathcal{R} = 1$ the fastest and such a small $\mathcal{R}$ has been found to give spectra steeper than $-5/3$ [Brethouwer et al., 2007]. The energy out of the cloud for all UIC and SIC cases where $N \neq 0$ is steeper than $-5/3$ is due to $\mathcal{R} < 1$ at all times in those regions [Brethouwer et al., 2007]. The large scale maximum of this energy particularly at small wavenumbers increases for larger N and it has even been observed that this energy becomes equivalent as that in the cloud. This is demonstrated in panel (d) of figure 3.23 which is the horizontal wavenumber energy spectra plot of the strongest stratification $N = 0.6$ used for all simulations performed in this thesis.

3.6.2 Vertical Spectra

This subsection is focused on analysing the vertical wavenumber spectra of the total energy within the cloud. This total energy is also defined here as the sum of the kinetic and potential energies. The total energy is used again for this spectral analysis, as with the

previous subsection, because it provides a great first approach in trying to understand the evolution of the spectra between the inhomogeneous and homogeneous turbulent systems. All plots in this subsection contain a line of slope -3 at the top right of all plots so as to be able to compare to the slope of the spectra at varying ranges of vertical wavenumbers.

Figure 3.25: Vertical wavenumber spectra of total energy within the cloud for $N = 0$ at (a) $t = 50$, (b) $t = 100$, (c) $t = 150$ and (d) $t = 200$.

Figure 3.25 shows the total vertical wavenumber energy spectra for the simulations with $N = 0$. The vertical spectra for $N = 0$ have the same shape and similar amounts of energy for the homogeneous and inhomogeneous simulations but as was seen in the horizontal spectra, the latter system also possesses less energy than its former counterpart. Panels (a)-(d) in figure 3.25 relay one noticeable characteristic of the spectra at all plotted times. It can be seen that for small wavenumbers, the spectra are shallower than -3 and then transitions to become much steeper than -3 at larger wavenumbers. This steepness is due to viscous effects at small enough scales so it can be said from figure 3.25 that the vertical spectra where $N = 0$ is shallower than -3 for all times. This is not surprising as this is the unstratified case, for which the k_v spectral slope should be closer to -5/3.
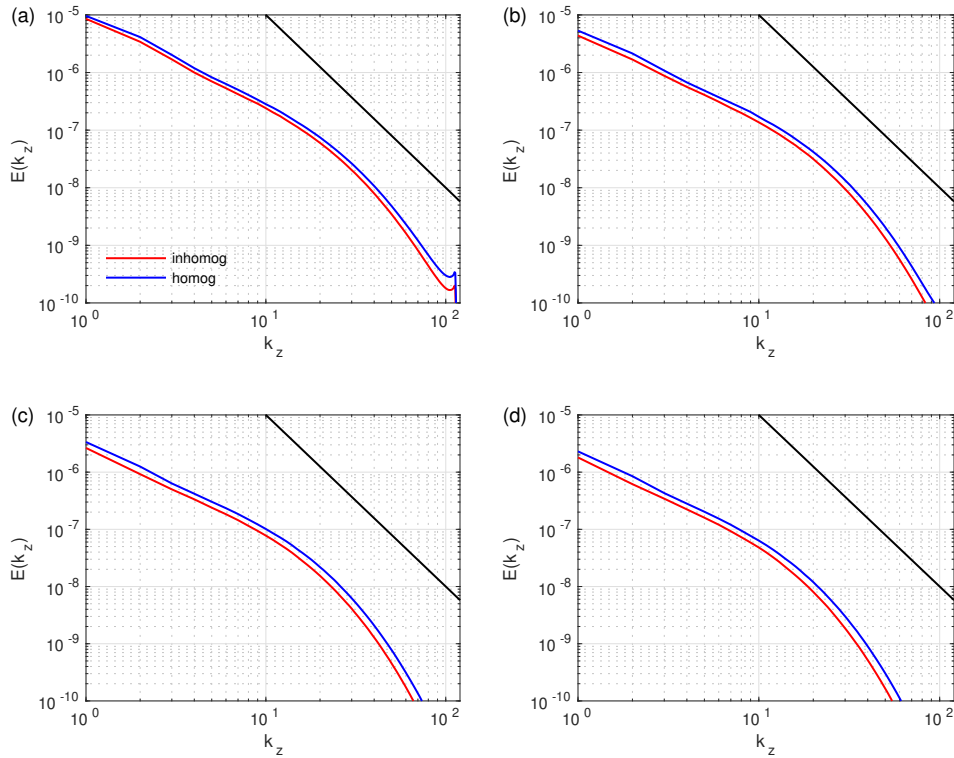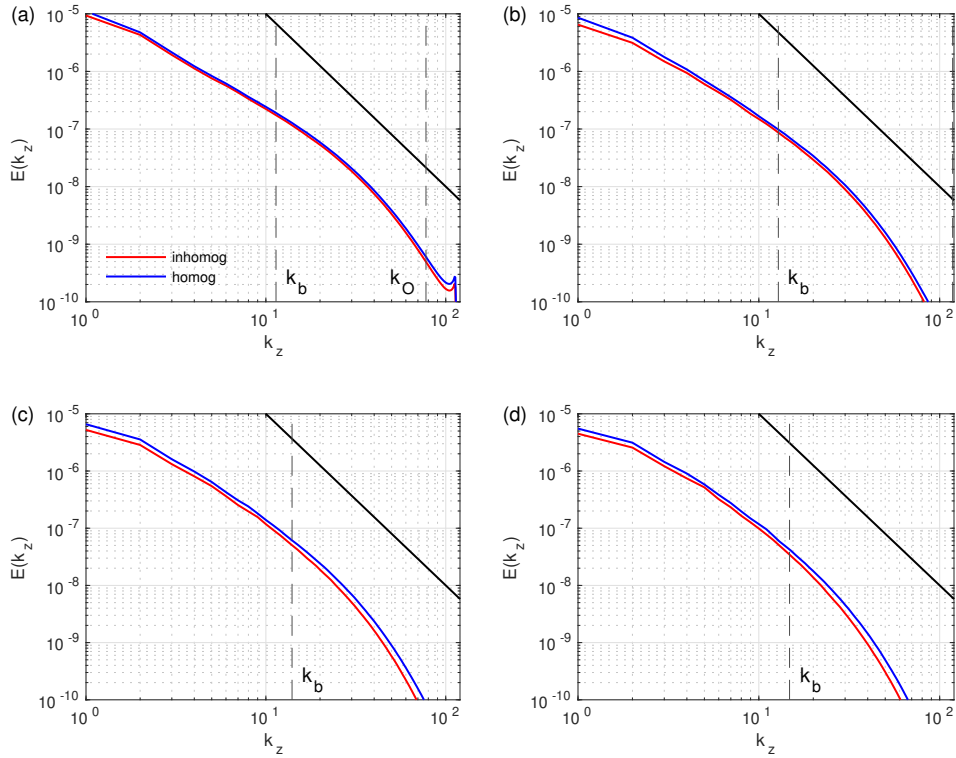
Figure 3.26: Vertical wavenumber spectra of total energy within the cloud for $N = 0.15$ at (a) $t = 50$, (b) $t = 100$, (c) $t = 150$ and (d) $t = 200$.

Figure 3.26 shows the total vertical wavenumber energy spectra for the simulations with $N = 0.15$. The energy in the homogeneous system is almost equivalent to that in the inhomogeneous system but with the latter having slightly less energy than the former over the full wavenumber range. This difference between the energy of these systems can be seen as later times in panels (c) and (d) where the inhomogeneous system presents itself as having slightly less energy by noticing the deviation from the homoegeneous curve at large wavenumbers. Upon inspection of all four panels in figure 3.26, the spectra at all times look shallower than -3 but is certainly steeper than the spectra in figure 3.25. It seems that as N increases, the slope of the spectra becomes closer to -3. At early times, the spectra in panel (a) is quite shallow and shows a transition to the steeper dissipation range at $k_z = 30 - 40$. As time progresses in panels (b)-(d), the spectra becomes steeper to have a slope of approximately -2. At best, where the spectra transitions between shallow and steep spectra, a tangent can be drawn with slope -3 but this does not indicate to a clear range of wavenumbers with a well defined slope..

Figure 3.27: Vertical wavenumber spectra of total energy within the cloud for $N = 0.3$ at (a) $t = 50$, (b) $t = 100$, (c) $t = 150$ and (d) $t = 200$.

Figure 3.27 shows the total vertical wavenumber energy spectra for the simulations with $N = 0.3$. A trend can be seen to form when comparing the spectra at small wavenumbers and large wavenumbers in figures 3.26 and 3.27. It appears that at small k_z, the spectra get shallower with increasing N and this can be seen particularly clearly by comparing panels (c) and (d) in both figures. Furthermore, at larger k_z with increasing N, the spectra get steeper and fall away quite quickly from the reference line of slope -3. A spectrum of slope -3 is expected for for $k_z > k_b$ but there is not enough of a range to see it in figure 3.27. One other comparison between figures 3.26 and figure 3.27 is that the spectra with larger N has a more parabolic shape than the other. This further emphasizes the increased shallowness and steepness of the spectra for small and large k_z respectively. Such a parabolic shape indicates that viscous effects are important and that there is no explicit constant slope especially between k_b and k_d to be compared to that of -3.

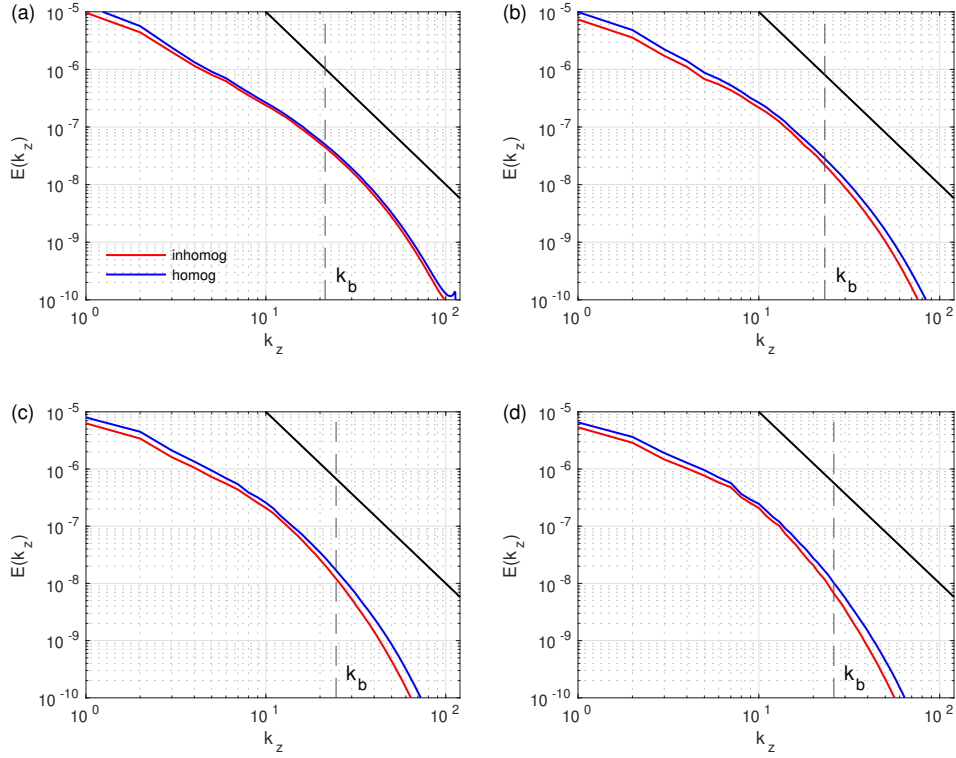Figure 3.28 shows the total vertical wavenumber energy spectra for the simulations with

Figure 3.28: Vertical wavenumber spectra of total energy within the cloud for $N = 0.6$ at (a) $t = 50$, (b) $t = 100$, (c) $t = 150$ and (d) $t = 200$.

$N = 0.6$. This case in which the stratification is the strongest shows at all times in panels (a)-(d) that the spectra is shallower than -3 at small k_z and quite steeper than -3 at large k_z. Panel (d) also has a more robust parabolic shape with a visible 'peak' when compared to same panels in figures 3.26 and 3.27 which also indicates to the greater shallow and steep slopes of the spectra at the small and large wavenumbers respectively. This 'peak' in the parabolic shape of the spectra also appears to occur at increasingly smaller wavenumbers for larger N when the same plots are compared. Furthermore, there is not enough of a range of wavenumbers beyond k_b to attempt any observation of the spectra having a -3 slope.

Figure 3.29 shows the total vertical wavenumber energy spectra for the simulations with $N = 0.3$(SIC). There is only a slight distinguishing factor between the homogeneous and inhomogeneous systems which means the energy between the two is roughly equivalent. However, an immediate observation can be appreciated in that this is the only figure in this
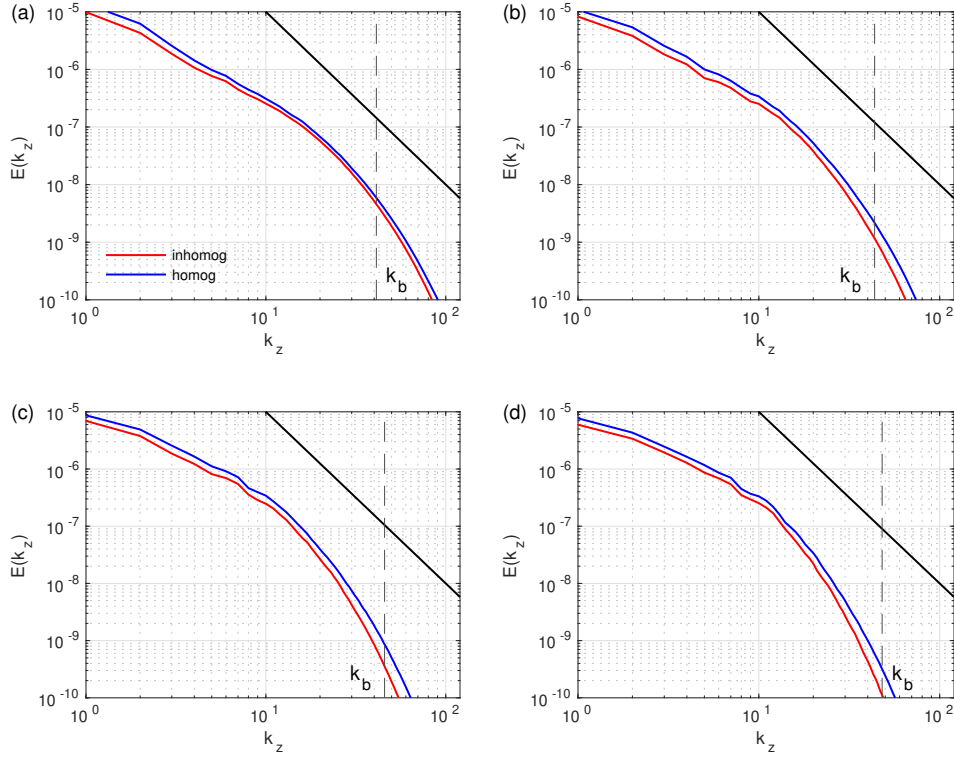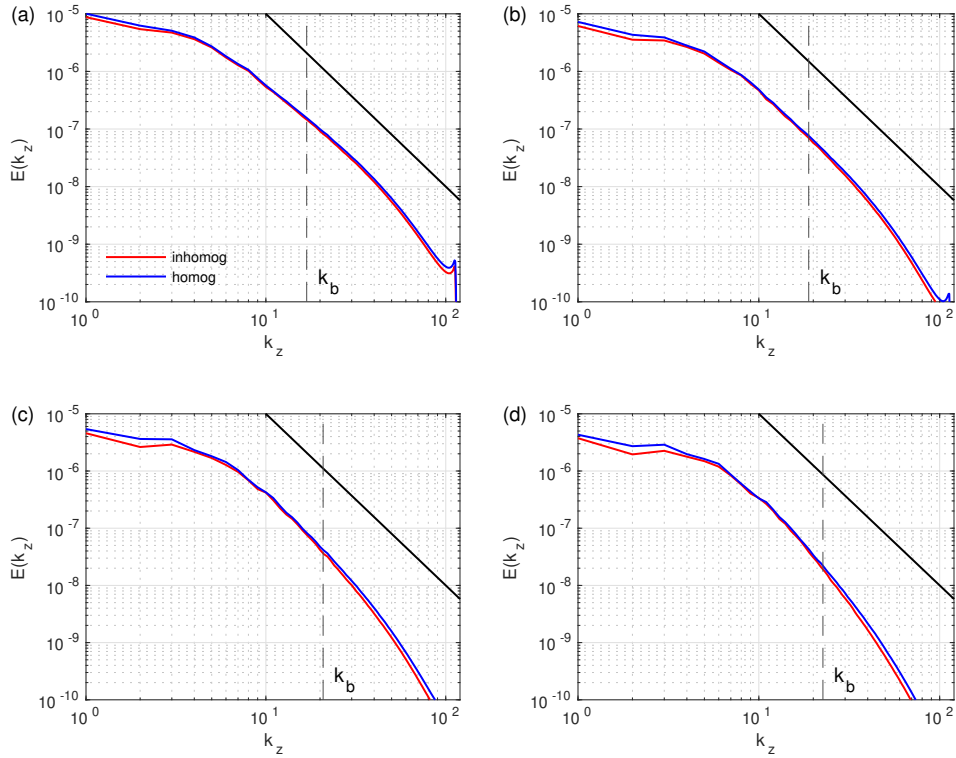
Figure 3.29: Vertical wavenumber spectra of total energy within the cloud for $N = 0.3$(SIC) at (a) $t = 50$, (b) $t = 100$, (c) $t = 150$ and (d) $t = 200$.

subsection where the spectra clearly agrees with the reference line of slope -3 for a defined range of wavenumbers. It is worth comparing figures 3.29 and 3.27 which both have $N = 0.3$ but are defined as SIC and UIC respectively. The immediate difference between them, as mentioned above, is that the SIC simulation has spectra has much better agreement to a -3 slope over a range of wavenumbers whereas the UIC simulation in its predominantly parabolic shape, does not. It is true that for both cases at small wavenumbers, the spectra is shallower than -3 but at $k_z > k_b$, only the SIC run achieves the -3 slope. It should also be noted that this -3 slope agreement with the SIC vertical spectra is evident for panels (a)-(c). In panel (d) with increasing time, the spectra falls away steeply from before the buoyancy wavenumber k_b.

It appears that there is an underlying importance on the initial conditions of the simulations as the results of the UIC or SIC cases vary significantly. The UIC simulations never achieved the -3 spectral slope and assumed a parabolic shape. Also, the UIC runs

have shallow spectra at small vertical wavenumbers and steep spectra at large vertical wavenumbers. There also was not a large enough range past the buoyancy wavenumber for a -3 spectral slope to exist. However, for the SIC case, the spectra had a clear agreement to the reference line of slope -3 in the buoyancy range for a substantial period of time. It seems as though the adjustment to the stratification plus the effect of the cloud inhibit the development of some of the expected features of stratified turbulence for the UIC simulations. However, when the initial conditions are already stratified turbulence, expected results are obtained which in this case is the -3 spectral slope of vertical wavenumber total energy, and they persist even as the cloud evolves. Thus, it appears that the initial conditions have a much more significant impact on the vertical wavenumber spectrum in the cloud than whether the turbulence is homogeneous or inhomogeneous.

3.7   Wave Angle Propagation

The section seeks to compare the theoretical and observed angles (from the previous section) of wave propagation in the regions above and below the clouds which are the parts of the domain that was originally quiescent at the beginning of the simulations. The graphs plotted in this section are ω_e vs k_h so as to utilise the relationship of $\omega_e = N\cos(\theta)$. As eddies often assist in the exciting of waves, calculating this eddy frequency using equation 2.19 is useful in finding the phase angle θ of waves propagated with a similar frequency. This θ is the angle of the wavevectors with the horizontal, however, the reference lines included in the physical space plots in the previous section use this same value of θ but from the vertical. The reasoning for this particular orientation of these angular reference lines is that the bands of the waves, which represent the crests and troughs, will be perpendicular to the wavevectors. Thus, these reference lines seek to give an idea of the expected orientation of the bands of crests and troughs.

Figure 3.30 shows the evolution of the eddy frequency scaled by the stratification such that $\omega_e/N = \cos(\theta)$. The portions of interest in figure 3.30 is the value of the curves at small horizontal wavenumbers, in particular, $k_h < 10$ as the largest amounts of energy within the eddies are located within this range. The action of these highly energetic eddies contribute to the exciting and propagation of waves in the regions outside of the cloud. Thus, by calculating the frequency of the most energetic eddies, an approximation of the frequency of the generated waves can be established and then the theoretical phase angle θ of those waves can be calculated.

For $N = 0.15$, a bump can be seen at $k_h = 3$ with $\omega_e/N = 0.2$. With the progress of time, this bump remains at the same wavenumber but its subsequent value goes down to
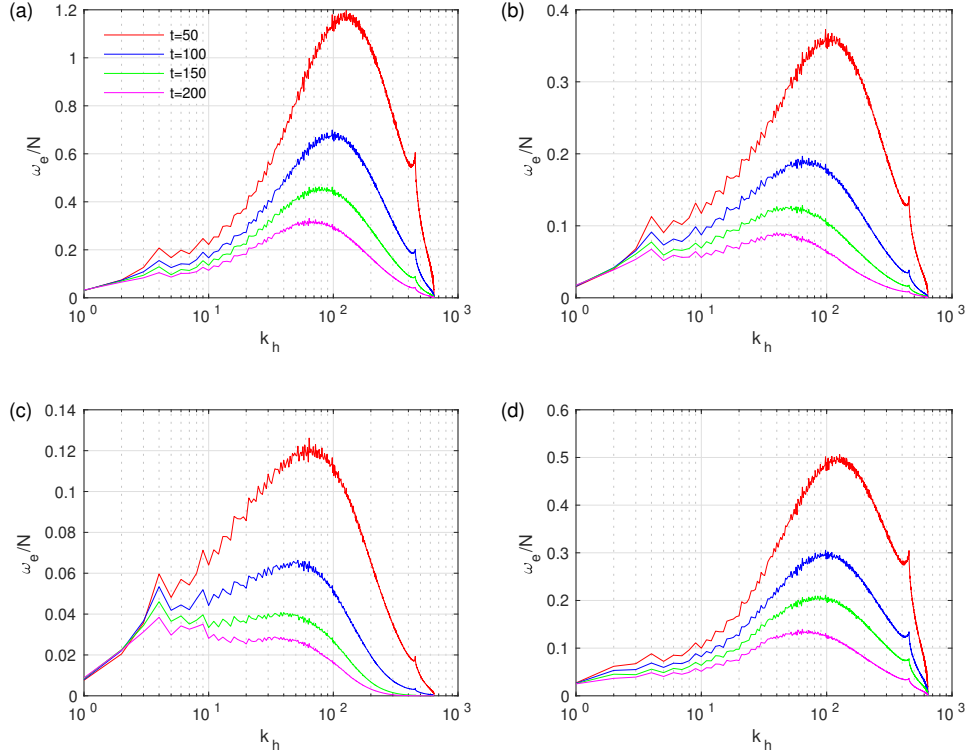
Figure 3.30: Angle of wave propagation for (a) $N = 0.15$, (b) $N = 0.3$, (c) $N = 0.6$ and (d) $N = 0.3$(SIC).

approximately 0.1. Taking the inverse cosine of these values gives a range of $78° - 84°$ for θ. For the other panels with N varying from (b) 0.3, (c) 0.6 and (d) 0.3(SIC), a similar bump in the plots occur at $k_h = 3$ with its amplitude decreasing with the evolution of time. The corresponding ω_e/N values of these shrinking bumps decrease with increasing N. It is between 0.075 and 0.1 for $N = 0.3$, between 0.04 and 0.06 for $N = 0.6$ and between 0.05 and 0.1 for $N = 0.3$(SIC). This gives angular ranges of $84° - 86°$, $86° - 87°$ and $84° - 87°$ respectively. It should also be pointed out that range of angles for $N = 0.3$(UIC) and $N = 0.3$(SIC) only differs by $1°$. Observing panels (b) and (d) in figure 3.30, there is a bigger difference between the amplitude of the $k_h = 3$ bumps for the SIC case than for the UIC case. This directly infers to the SIC case having a larger range of θ than the UIC case. Furthermore, referring back to the potential temperature perturbation figures 3.15 and 3.19, the former UIC case had shown stronger wave activity outside of the cloud when compared to the latter SIC case. This indicates that the narrower range of the UIC case has a stronger wave presence out of the cloud with respect to the SIC case. Such a

result is due to the response of the UIC simulation having stratification being applied to initially unstratified turbulence whereas the SIC simulation continued its evolution from its initially stratified turbulence.

Given that the ranges of angles for wave propagation have been calculated theoretically for various N, a comparison to the observed angles in the potential temperature perturbations figures from the previous section is required to justify results. For potential temperature figures with $N = 0.3$ and $N = 0.6$, there are bands near to the cloud's boundaries that roughly agree with the respective range of angles calculated for a particular N. However, there is also significant wave presence in the upper and lower extremities of the domain discussed above due to the arrangement of the bands in the vorticity plots and patches in the potential temperature plots which do not match with the computed angles. This discrepancy can be explained by invoking the definition of group velocity. For large θ that is close to $90°$ as with the current cases of large N, the wavevector is almost vertical. This means that the group velocity is almost horizontal [Kundu et al., 2012] and the wave energy is unable to propagate far away from the cloud. In fact, this direction of propagation is also almost parallel to the cloud. However, higher frequency waves with smaller θ have more vertically oriented group velocity. Therefore, even though the higher frequency waves may be less energetic as they are excited by lower energy eddies, they are the waves that are able to propagate away from the cloud and can be seen to extend as far towards the fringes of the domain. This point is emphasized for the $N = 0.3$ UIC and SIC simulations. The former had significantly more wave presence if focus is particularly placed on the edges of the cloud when comparing figures 3.15 and 3.19. This corresponds to the narrower angular range of the UIC simulation which infers that the wider angular range of the SIC simulation should have slightly more vertically oriented group velocity. The arrangement of the bands in figure 3.18 and patches in figure 3.19 at the upper and lower ends of the domain indicates that there is indeed some wave activity far away from the cloud.

Chapter 4

Summary and Conclusions

This thesis seeks to offer a detailed comparison between homogeneous and inhomogeneous turbulence via direct numerical simulations carried out in a cubic domain. Homogeneous turbulence studies have been performed for a myriad of initialized conditions, forcing parameters and varying of stratification that influences the particular system. An equivalent analysis put forward in studying homogeneous turbulence is not present for that of inhomogeneous turbulence. Within this study, the initial conditions on the system of inhomogeneous and homogeneous turbulence are taken from simulations of forced turbulence [Lang and Waite, 2019], with and without stratification. It is of great hope that this serves as a starting point for more advanced studies in the foreseeable future.

The inhomogeneous turbulence is defined as a turbulent cloud in a cubic domain with a defined height in the z-direction where above and below this cloud are quiescent regions. Characteristics emerging from this system of turbulence in the cloud are then compared to those of homogeneous turbulence which fill another domain of the same size. Analysis was then performed on the inhomogeneous turbulent cloud and then compared to a similarly demarcated cloud region for the homogeneous system. This comparison strives to highlight any distinguishing traits of the inhomogeneous system and this is labelled as that which is 'in the cloud'. As time evolves, the boundaries of the cloud become ambiguous and the region labelled as 'out of the cloud' is more restricted to the upper and lower parts of the domain that what was defined at the beginning of the simulations. Four of the simulations possessed initial conditions taken from an unstratified simulation with $N = 0$ [Lang and Waite, 2019] with the fifth one having a different value of $N = 0.3$(SIC).

For this comparison between homogeneous and inhomogeneous turbulence, several criteria were studied and analysed. These include energy time series (kinetic, potential, vortex

and wave), vertical and horizontal Froude numbers, buoyancy Reynolds number, dissipation, temporal changes of energy (kinetic, potential, vortex and wave) within the cloud, wave angle propagation, internal wave activity outside of the cloud and computing both the horizontal and vertical energy spectra. All of these are examined whilst also varying the degree of stratifications of the simulations.

In general, the inhomogeneous simulations experience greater decay than the homogeneous simulations for the energy time series. However, the decay is not significant enough to offer a stark difference between the simulations and the energies in both system are quantitatively similar. Horizontal Froude numbers were found to be less than 1 which is indicative and the presence of strong stratification. However, the vertical Froude numbers decrease with increasing N rather than maintaining the relationship $Fr_v \sim O(1)$. This is a new result as it is expected that doubling N should halve the vertical length scale l_v which is necessary to keep $Fr_v \sim O(1)$. Upon inspection of l_v calculated in this thesis, it remains within a narrow band of values with varying N. With this result, it appears that the turbulence in the cloud adjusts to both stratification as well as the cloud and it is unable to develop smaller length scales with $Fr_v \sim 1$ before decaying.

The buoyancy Reynolds number $\mathcal{R}$ for all N at initial time started above 1. With the evolution of time, all simulations eventually dipped to $\mathcal{R} \sim 1$ with the exception of the $N = 0.6$ run which achieved $\mathcal{R} < 1$ at extremely early times in the simulation. Moreover, as N increases, the simulations reached or breached that threshold value of $\mathcal{R} = 1$ in shorter periods of time. This decrease of $\mathcal{R}$ with time coincides with ranges of wavenumbers to which the horizontal and vertical spectra are $-5/3$ and -3 respectively. The general trend for those simulations with initial condition of $N = 0$ is that the range of wavenumbers which correspond to power-law gradients $-5/3$ and -3 moves to smaller wavenumbers for increasing time. In addition to this feature, this receding range also shrinks for increasing N. However, the simulation with initial condition $N = 0.3$(SIC) boasts the largest range of the spectra coinciding with $-5/3$ and -3 and maintains this with progressing time.

Another feature of interest in this study was the increasing presence of waves in the regions outside of the cloud accompanied by a corresponding decrease of both potential and wave energies inside the cloud (figures 3.3 and 3.5). Energy time series showed a definite increase in potential and wave energies outside of the cloud with kinetic and vortex energy remaining localized within the cloud. Moreover, physical space plots of the second component of vorticity and potential temperature indicate heavily to the presence of such internal waves above and below the cloud. Furthermore, larger N promotes greater activity outside the cloud in shorter periods of time. It was only natural to continue this exciting development by attempting to calculate the angles by which these waves have propagated. Using the eddy frequency of the strongest eddies to find the frequency of waves encouraged

by them, the range of angles find themselves in quasi-horizontal ranges between $76° - 89°$. Such large values of the phase angle θ point to almost vertical wavevectors and subsequently almost horizontal group velocity. Thus, the waves moving with such a group velocity does not propagate away from the cloud but in a direction near and parallel to it. This can be seen at later times in figures 3.14-3.18 and 3.15-3.19 where the bands of vorticity and patches of potential temperature near the edges of the cloud are in good agreement to the the angular reference lines.

Inhomogeneous turbulence is establishing its seat at the royal but overcrowded table of its homoegeneous turbulence ancestors. Recent examples of inhomogeneous turbulence involve 1) analyzing the evolution of various stratified cloud orientations [Maffioli et al., 2014] and 2) investigating wake evolution dynamics along with internal wave angle propagation for an object being towed through a stratified cloud [Rowe et al., 2020]. Future work that can be pursued from the research done in this thesis can include and is certainly not limited to

- an incorporation of forcing into a single inhomogeneous stratified cloud and observe its spectral evolution with time to possibly confirm a wider range of wavenumbers that relate to slopes of $-5/3$ and -3,

- having multiple variably sized stratified clouds in a defined domain, with or without forcing, and thoroughly explore their behaviour and interactions amongst each other,

- investigate the effect(s) of the size of the cloud,

- simulate bigger domains so there is more room outside the cloud,

- remove the assumption of a constant stratification N^2,

- any combination of the above.

References

A. M. Abdilghanie and P. J. Diamessis. The internal gravity wave field emitted by a stably stratified turbulent wake. *Journal of Fluid Mechanics*, 720:104–139, 2013.

S. Almalkie and S. M. de Bruyn Kops. Kinetic energy dynamics in forced, homogeneous, and axisymmetric stably stratified turbulence. *Journal of Turbulence*, 13(13):N29, 2012.

P. Augier, J.-M. Chomaz, and P. Billant. Spectral analysis of the transition to turbulence from a dipole in stratified fluid. *Journal of Fluid Mechanics*, 713:86–108, 2012.

P. Bartello. Geostrophic adjustment and inverse cascades in rotating stratified turbulence. *Journal Of The Atmospheric Sciences*, 52(24):4410–4428, 1995.

P. Billant and J.-M. Chomaz. Experimental evidence for a new instability of a vertical columnar vortex pair in a strongly stratified fluid. *Journal Of Fluid Mechanics*, 418:167–188, 2000a.

P. Billant and J.-M. Chomaz. Theoretical analysis of the zigzag instability of a vertical columnar vortex pair in a strongly stratified fluid. *Journal Of Fluid Mechanics*, 419:29–63, 2000b.

P. Billant and J.-M. Chomaz. Three-dimensional stability of a vertical columnar vortex pair in a stratified fluid. *Journal Of Fluid Mechanics*, 419:65–91, 2000c.

P. Billant and J.-M. Chomaz. Self-similarity of strongly stratified inviscid flows. *Physics of Fluids*, 13(6):1645–1651, 2001.

G. Brethouwer, P. Billant, E. Linborg, and J.-M. Chomaz. Scaling analysis and simulation of strongly stratified turbulent flows. *Journal Of Fluid Mechanics*, 585:343–368, 2007.

G. F. Carnevale, M. Briscolini, and P. Orlandi. Buoyancy- to inertial-range transition in forced stratified turbulence. *Journal Of Fluid Mechanics*, 427:205–239, 2001.

P. A. Davidson. *Turbulence: An Introduction For Scientists And Engineers.* Oxford University Press, Oxford, 2004.

K. J. Devlin. *The Millennium Problems: The Seven Greatest Unsolved Mathematical Puzzles Of Our Time.* Basic Books, New York, 2002.

K. Dohan and B. R. Sutherland. Internal waves generated from a turbulent mixed region. *Physics of Fluids*, 15(2):488–498, 2003.

J. P. Dougherty. The anisotropy of turbulence at the meteor level. *Journal Of Atmospheric And Terrestrial Physics*, 21(2):210–213, 1961.

D. R. Durran. *Numerical Methods For Fluid Dynamics With Applications To Geophysics.* Springer, New York, 2nd ed. edition, 2010.

P. He and S. Basu. Direct numerical simulation of intermittent turbulence under stably stratified conditions. *Nonlinear Processes In Geophysics*, 22(4):447–471, 2015.

D. A. Hebert and S. M. de Bruyn Kops. Relationship between vertical shear rate and kinetic energy dissipation rate in stably stratified flows. *Geophysical Research Letters*, 33(6):L06602, 2006.

J. R. Herring and O. Métais. Numerical experiments in forced stably stratified turbulence. *Journal Of Fluid Mechanics*, 202:97–115, 1989.

Y. Kimura and J. R. Herring. Energy spectra of stably stratified turbulence. *Journal Of Fluid Mechanics*, 698:19–50, 2012.

Y. Kitamura and Y. Matsuda. The k_h^{-3} and $k_h^{-5/3}$ energy spectra in stratified turbulence. *Geophysical Research Letters*, 33(5):L05809, 2006.

A. N. Kolmogorov. Dissipation of energy in the locally isotropic turbulence. *Dokl. Akad. Nauk SSSR*, 32(1), 1941a.

A. N. Kolmogorov. The local structure of turbulence in incompressible viscous fluid for very large Reynolds numbers. *Dokl. Akad. Nauk SSSR*, 30(4), 1941b.

R. H. Kraichnan. Inertial ranges in two-dimensional turbulence. *The Physics of Fluids*, 10(7):1417–1423, 1967.

P. K. Kundu, I. M. Cohen, and D. R. Dowling. *Fluid Mechanics.* Academic Press, Waltham, MA, 5th ed. edition, 2012.

C. J. Lang and M. L. Waite. Scale-dependent anisotropy in forced stratified turbulence. *Physical Review Fluids*, 4(4), 2019.

J. D. Legaspi. Prandtl number dependence of stratified turbulence. Master's thesis, University of Waterloo, Waterloo, ON, 2019.

J. D. Legaspi and M. L. Waite. Prandtl number dependence of stratified turbulence. *Journal Of Fluid Mechanics*, 903:A12, 2020.

E. Lindborg. The energy cascade in a strongly stratified fluid. *Journal Of Fluid Mechanics*, 550(1):207–242, 2006.

A. Maffioli. Vertical spectra of stratified turbulence at large horizontal scales. *Physical Review Fluids*, 2(10), 2017.

A. Maffioli and P. A. Davidson. Dynamics of stratified turbulence decaying from a high buoyancy Reynolds number. *Journal Of Fluid Mechanics*, 786:210–233, 2016.

A. Maffioli, P. A. Davidson, S. B. Dalziel, and N. Swaminathan. The evolution of a stratified turbulent cloud. *Journal Of Fluid Mechanics*, 739:229–253, 2014.

L. Mahrt. Intermittency of atmospheric turbulence. *Journal Of The Atmospheric Sciences*, 46(1):79–95, 1989.

R. V. Ozmidov. On the turbulent exchange in a stably stratified ocean. *Atmospheric And Oceanic Physics*, 1:493, 1965.

S. B. Pope. *Turbulent Flows*. Cambridge University Press, Cambridge, 2000.

L. F. Richardson. *Weather Prediction By Numerical Process*. Dover Publications, New York, 1965.

J. J. Riley and S. M. deBruynKops. Dynamics of turbulence strongly influenced by buoyancy. *Physics Of Fluids*, 15(7):2047–2059, 2003.

J. J. Riley and M.-P. Lelong. Fluid motions in the presence of strong stable stratification. *Annual Review Of Fluid Mechanics*, 32(1):613–657, 2000.

J. J. Riley and R. W. Metcalfe. Direct numerical simulations of turbulent patches in stably-stratified fluids. In *Proc. Of The 3rd International Symposium On Stratified Flows*, Stratified Flows I, California Institute of Technology, Pasadena, 1987.

K. L. Rowe, P. J. Diamessis, and Q. Zhou. Internal gravity wave radiation from a stratified turbulent wake. *Journal Of Fluid Mechanics*, 888, 2020.

W. D. Smyth and J. N. Moum. Anisotropy of turbulence in stably stratified mixing layers. *Physics Of Fluids*, 12(6):1343–1362, 2000a.

W. D. Smyth and J. N. Moum. Length scales of turbulence in stably stratified mixing layers. *Physics Of Fluids*, 12(6):1327–1342, 2000b.

H. Tennekes and J. L. Lumley. *A First Course In Turbulence*. MIT Press, Cambridge, Mass, 1972.

M. L. Waite. Stratified turbulence at the buoyancy scale. *Physics Of Fluids*, 23(6):066602–066602–12, 2011.

M. L. Waite. Potential enstrophy in stratified turbulence. *Journal Of Fluid Mechanics*, 722:R41–R411, 2013.

M. L. Waite and P. Bartello. Stratified turbulence dominated by vortical motion. *Journal Of Fluid Mechanics*, 517:281–308, 2004.

J. C. Wyngaard. *Turbulence In The Atmosphere*. Cambridge University Press, Cambridge, UK, 2010.

Q. Zhou and P. J. Diamessis. Large-scale characteristics of stratified wake turbulence at varying Reynolds number. *Physical Review Fluids*, 4(8), 2019.